Aus der Klinik für Radioonkologie und Strahlentherapie
der Medizinischen Fakultät Charité – Universitätsmedizin Berlin

DISSERTATION

Differentiation of Tumor Recurrence from Radionecrosis Using ^{18}F-FET-PET/CT after CyberKnife Radiosurgery of Brain Tumors

Differenzierung zwischen Tumorrezidiv und Radionekrose mittels ^{18}F-FET-PET/CT nach radiochirurgischer Behandlung von Hirntumoren mit dem CyberKnife

zur Erlangung des akademischen Grades
Doctor medicinae (Dr. med.)

vorgelegt der Medizinischen Fakultät
Charité – Universitätsmedizin Berlin

von

Winna Lim
aus Medan, Indonesien

Datum der Promotion: 30. November 2023

Preface

Parts of this monograph have been published in the international peer-reviewed journal *Cancer Treatment and Research Communications*. The results reported in this publication are based on data collected as part of this dissertation.

Lim W, Acker G, Hardt J, Kufeld M, Kluge A, Brenner W, Conti A, Budach V, Vajkoczy P, Senger C, Prasad V. Dynamic ^{18}F-FET PET/CT to differentiate recurrent primary brain tumor and brain metastases from radiation necrosis after single-session robotic radiosurgery. Cancer Treat Res Commun. 2022;32:100583. doi: 10.1016/j.ctarc.2022.100583. Epub 2022 Jun 3. PMID: 35688103.

Initial results of this work were presented as a poster at the *57. Jahrestagung der Deutschen Gesellschaft für Nuklearmedizin* (57th Annual Meeting of the German Society of Nuclear Medicine) on April 4, 2019.

W. Winna, M. Kufeld, J. Hardt, C. Senger, A. Conti, V. Budach, W. Brenner, V. Prasad. Retrospective Analysis of Differentiation of Suspected Brain Lesions after CyberKnife® Radiosurgery using Dynamic ^{18}F-FET-PET and MRI. Poster contribution.

Table of Contents

List of Figures

List of Tables

Abbreviations

BED	Biologically equivalent dose
CNS	Central nervous system
CK	CyberKnife®
CK-RS	CyberKnife® radiosurgery
cMRI	Cranial MRI
CT	Computed tomography
FET	O-(2-[18F]fluoroethyl)-l-tyrosine
GTV	Gross tumor volume
METS	Group of metastatic brain lesions in the study population
MRI	Magnetic resonance imaging
MP-RAGE	Magnetization-Prepared Rapid Acquisition Gradient Echo
PET	Positron emission tomography
PBT	Primary brain tumor
PTV	Planning target volume
ROI	Region of interest
RT	Radiotherapy
SBT	Secondary brain tumor
SRS	Stereotactic radiosurgery
SUV	Standardized uptake value
SUVmax	Maximum standardized uptake value
SUVmean	Mean standardized uptake value
TAC	Time-activity curve
TBR	Tumor-to-background ratio
TBRmax	Maximum tumor-to-background ratio
TBRmean	Mean tumor-to-background ratio
TOTAL	Group of all primary and secondary brain lesions in the study population
TTP	Time to peak
vs.	versus
WBRT	Whole brain radiotherapy
WHO	World Health Organization

Abstract

BACKGROUND: ^{18}F-FET-positron emission tomography/computed tomography (FET-PET) has reliable diagnostic accuracy in differentiating recurrent brain tumor from radionecrosis after radiosurgery. This explorative study analyzed this role of FET-PET in brain tumors treated by image-guided robotic stereotactic radiosurgery using CyberKnife® (CK-RS).

METHOD: The study population were patients who underwent FET-PET to resolve inconclusive magnetic resonance imaging (MRI) findings in the clinical follow-up of primary and secondary brain lesions after CK-RS in 2011-2017. Histology reports or best supporting clinicoradiological evidence served as reference standard. Static (tumor-to-background ratio [TBR]) and dynamic (time to peak [TTP] and time-activity curve [TAC] pattern) parameters were determined. Three TAC patterns were distinguished: continuously ascending curve (I), ascending curve followed by plateau (II), and steep ascent followed by slow descent (III). Receiver operating characteristic curve analysis and diagnostic accuracy tests were performed. Analyses were performed for all lesions (TOTAL) and brain metastases only (METS). MRI lesions not detected by FET-PET were qualitatively analyzed.

RESULTS: Fourteen patients (median 52 years, range 16-79 years) with a total of 28 lesions (5 primary brain tumor lesions in 2 patients and 23 metastases in 12 patients) were included. The median time interval between CK-RS and FET-PET was 10 months (range 4-35). Histology was available for 7/28 lesions (25%), all correctly diagnosed by FET-PET. TBRs were higher in recurrent tumor than radionecrosis (median TBR_{max} of 5.5 vs. 3.8 in TOTAL and 5.0 vs. 3.5 in METS; median TBR_{mean} of 2.6 vs. 2.1 in TOTAL and 2.4 vs. 2.0 in METS). Mean TTP was shorter in tumors (9.6 vs. 16.7 min in TOTAL and 8.3 vs. 13.7 min in METS) while median TTP did not differ. No significant cut-offs for TBR and TTP were found, thus published cut-offs of 1.95 for TBR_{mean} and 20 min for TTP were used. The best diagnostic accuracy was achieved for combined TBR_{mean} and TAC: TOTAL (METS): 75% (75%) sensitivity, 63% (71%) specificity, and 71% (74%) accuracy. When only TAC patterns were used, accuracy was 82% in TOTAL and 87% in METS. Post-test diagnostic probability was 12% (TOTAL) and 16% (METS) higher than that of follow-up MRI. Three lesions without PET tracer uptake were stable over time.

CONCLUSION: This explorative study shows that the best diagnostic accuracy of FET-PET in differentiating brain tumor recurrence from radionecrosis after CK-RS is achieved when combined static and dynamic parameters are used, resulting in up to 16% higher diagnostic probability than standard follow-up MRI.

Abstract

HINTERGRUND: Die ^{18}F-FET-Positron-Emissions-Tomographie/Computertomographie (FET-PET) weist eine verlässliche diagnostische Genauigkeit in der Differenzierung von Hirntumorrezidiven und Radionekrosen nach radiochirurgischer Behandlung auf. In dieser explorativen Studie wurde diese Rolle der FET-PET bei Hirntumoren nach bildgesteuerter robotergestützter stereotaktischer Radiochirurgiebehandlung mittels CyberKnife® (CK-RS) analysiert.

METHODIK: Eingeschlossen wurden Patienten, die sich von 2011 bis 2017 einer FET-PET-Untersuchung zur Abklärung unklarer magnetresonanztomographischer (MRT) Befunde im Rahmen der klinischen Nachsorge von primären und sekundären Hirnläsionen nach CK-RS unterzogen. Als Referenzstandard dienten Histologiebefunde oder klinisch-radiologische Befunde als *Best Supporting Evidence*. Statische (*Tumor-to-Background Ratio* [TBR]) und dynamische (*Time to Peak* [TTP] und *Time-Activity Curve* [TAC]) Parameter wurden ermittelt. Es wurden drei TAC-Muster unterschieden: kontinuierlich ansteigende Kurve (I), ansteigende Kurve mit nachfolgendem Plateau (II), und steil ansteigende Kurve mit flachem Abfall (III). Grenzwertoptimierungskurven wurden berechnet und diagnostische Genauigkeitstests durchgeführt. Analysen erfolgten für sämtliche Läsionen (TOTAL) sowie Hirnmetastasen (METS). Im MRT detektierte Läsionen, die nicht in der FET-PET abgrenzbar waren, wurden qualitativ analysiert.

ERGEBNISSE: Vierzehn Patienten (Medianalter 52 Jahre, Spannweite 16-79 Jahre) mit insgesamt 28 Hirnläsionen (5 primären Hirntumorläsionen in 2 Patienten und 23 Hirnmetastasen in 12 Patienten) wurden eingeschlossen. Die Medianzeit zwischen CK-RS und der FET-PET betrug 10 Monate (Spannweite 4–35 Monate). Ein histopathologischer Befund lag bei 7 von 28 Läsionen (25%) vor, die sämtlich mit der FET-PET korrekt diagnostiziert wurden. Die TBR war bei Hirntumorrezidiven höher als bei Radionekrosen (Median TBR_{max} TOTAL 5,5 vs. 3,8; METS 5,0 vs. 3,5; Median TBR_{mean} TOTAL 2,6 vs. 2,1; METS 2,4 vs. 2,0). TTP war im Mittel bei Hirntumoren kürzer (TOTAL 9,6 vs. 16,7 min; METS 8,3 vs. 13,7); die mediane TTP unterschied sich jedoch nicht. Signifikante TBR- und TTP-Grenzwerte ließen sich nicht berechnen, daher kamen eine in früheren Studien etablierte TBR_{mean} von 1,95 sowie eine TTP von 20 min zur Anwendung. Die besten diagnostichen Genauigkeitswerte fanden sich für die

Kombination von TBR_{mean} und TAC: TOTAL (METS): 75% (75%) Sensitivität, 63% (71%) Spezifizität und 71% (74%) Genauigkeit. Bei der alleinigen Betrachtung der TAC-Muster war die Genauigkeit 82% (TOTAL) bzw. 87% (METS). Die Nachtestdiagnosewahrscheinlichkeit war 12% (TOTAL) bzw. 16% (METS) höher als die der vorangehenden MRT-Untersuchung. Drei in der FET-PET nicht nuklidavide Läsionen waren im Verlauf stabil.

SCHLUSSFOLGERUNG: Die beste diagnostische Genauigkeit der FET-PET in der Unterscheidung von Hirntumorrezidiven und Radionekrosen nach CK-RS ergibt sich in der vorgestellten explorativen Studie für die Kombination von statischen und dynamischen Parametern. Hierdurch wird eine bis zu 16% höhere Diagnosewahrscheinlichkeit im Vergleich zur herkömmlichen Nachsorge-MRT erzielt.

1. Introduction

This introduction briefly addresses interdisciplinary topics relevant to this dissertation and includes an overview of malignant brain tumors and their management, an outline of the techniques of radiosurgery in general and CyberKnife in particular, and a discussion of the role of positron emission tomography (PET) in neuro-onocological imaging.

1.1. Overview of Tumors of the Central Nervous System

Central nervous system (CNS) tumors are a heterogeneous group of neoplasms. Their management is complex and challenging. Guidelines and research papers typically deal with either primary or secondary brain tumors (metastases). This section provides a general overview of both primary and secondary malignant brain tumors including their diagnosis and management.

1.1.1. Epidemiology

Brain tumors comprise malignant tumors that originate from different CNS cells (primary brain tumors, PBTs) and metastatic tumors that spread to the brain from primaries elsewhere in the body (secondary brain tumors, SBTs). The most recent data from the Central Brain Tumor Registry of the United States (CBTRUS), the largest registry providing population-based data on tumors of this kind, show an average annual age-adjusted incidence rate of approximately 7.1 per 100,000 population for malignant brain and other CNS tumors for the years 2014 to 2018 (2). Glioblastoma is the most frequent malignant PBT (2), and brain metastasis is the most common intracranial tumor in adults. Nevertheless, the exact epidemiology of SBTs is not known (3), and published data vary. For instance, brain metastases were found to be about three times more common than malignant PBTs in the United States in 2007, affecting approximately 6% of patients diagnosed with cancer in that year (4). Several other sources estimate that approximately 8-10% of cancer patients have symptomatic brain metastases, with supposedly hidden and higher numbers found at autopsy (5-7). The authors of a population-based study for the years 2010 through 2013 reported that 2% of all cancer patients had brain metastases at diagnosis and estimated the annual incidence of brain metastases in the United States to be more than 23,500 cases per year (8). Although many types of primary cancers will

eventually spread to the brain, the five most common primaries metastasizing to the brain are lung, skin, renal, breast, and colorectal cancers (4, 9). For these five cancers, two population-based studies conducted in Maastricht and Detroit reported similar incidences, ranging from 1.2% for colorectal cancer to 16.3% for lung cancer in Maastricht (7) and from 1.8% to 19.9%, respectively, in Detroit, with a combined incidence proportion of these five primaries of approximately 9.6% (6). Survival rates of patients with primary brain tumors depend on many factors, such as age, site within the brain, tumor aggressiveness, and tumor molecular properties. Malignant primary brain tumors have 5-year survival rates of about 35% (2, 10).

1.1.2. Classification

Before the 2016 World Health Organization (WHO) Classification of CNS Tumors, primary brain tumors were classified using histological and/or pathological features (11). As a result, for instance, all phenotypically astrocytic tumors were grouped separately from oligodendroglial phenotypes. The 2016 WHO classification additionally takes molecular genetic parameters into account in defining tumor entities (12). Some entities were thus newly recognized while others have been omitted from the classification. In the current 2021 WHO classification, a greater emphasis on molecular characteristics are placed in both tumor grading and tumor classification, leading to some diagnoses to be assessed totally based on their molecular features (13, 14). Terminologies were also partly changed. However, despite the updates throughout the years, the classification is still structured based on the origins of tumor cells. Table 1 lists the simplified version of major brain tumor classes distinguished in the current WHO classification.

1.1.3. Diagnosis

The clinical presentation of brain tumors depends on various factors including their location and growth rate. Symptoms can be focal or generalized and include headaches, seizures, nausea and vomiting, and neurological symptoms. The latter depend on affected cranial nerves and/or functional brain areas (15). Magnetic resonance imaging (MRI) is the method of choice for diagnostic workup in patients with signs and symptoms suggesting a brain tumor. The standard MRI protocol can be supplemented by multimodal functional pulse sequences such as MR spectroscopy and MR perfusion. Other important

imaging modalities are computed tomography (CT) and positron emission tomography (PET) (5, 16). If initial imaging findings suggest a brain metastasis and the patient has no history of cancer, a thorough systemic cancer screening including CT of the chest and abdomen and/or (18)F-fluorodeoxyglucose (FDG-)PET will follow to locate the primary tumor. Whenever these imaging modalities do not yield a definitive diagnosis and in patients with cancer of unknown primary (CUP), a tissue sample should be obtained before therapy, either through stereotactic biopsy or open surgery (16). Biopsy should also be considered when the suspicious brain lesion appears to be atypical for a certain diagnosis (of primary tumor) or when a long time has elapsed since cancer was first diagnosed in a patient (16).

Table 1. Simplified classification of brain tumors

Major Classes of Brain Tumors*

• Gliomas, glioneuronal tumors, and neuronal tumors
  ○ Adult-type diffuse gliomas
  ○ Pediatric-type diffuse gliomas
  ○ Circumscribed astrocytic gliomas
  ○ Glioneuronal and neuronal tumors
  ○ Ependymal tumors
• Choroid plexus tumors
• Embryonal tumors
• Pineal tumors
• Cranial and paraspinal nerve tumors
• Meningiomas
• Mesenchymal, non-meningothelial tumors
• Melanocytic tumors
• Hematolymphoid tumors
• Germ cell tumors
• Tumors of the sellar region
• Metastatic tumors

*Simplified and adapted from the 2021 WHO Classification of Tumors of the CNS (13).

1.1.4. Principles of CNS Tumor Management

The main treatments in neuro-oncology are surgery, radiotherapy, and systemic treatment (Figure 1). Further medical management includes symptomatic treatment of mass effects (caused by tumor, edema, or radiation necrosis), seizures, endocrine disorders, fatigue, mood and cognitive disorders, as well as venous thromboembolism (5), all of which can occur in both primary and secondary brain tumors (17, 18).

The initial key treatment in neuro-oncology is neurosurgical resection because it lowers the mortality rate in all glioma types, prolongs survival, improves quality of life by improving functional status, and may be the sole curative option, for example, in pediatric cases (5, 15, 19-21). Radiotherapy is a further essential element of brain tumor management and is done either in an adjuvant setting after surgery or as stand-alone therapy in patients who are not candidates for surgery. Radiotherapy in neuro-oncology

includes fractionated external beam radiation therapy, radiosurgery, brachytherapy, intraoperative radiotherapy, and targeted radionuclide therapy (22).

Systemic treatment options available to brain tumor patients include cytotoxic alkylating chemotherapy and antiangiogenic therapy, as well as immunotherapy in patients with metastatic brain tumors or malignant gliomas (5). Many cancer immunotherapies such as cancer vaccines (23, 24), oncolytic virotherapeutics (25, 26), checkpoint inhibitors (27), adoptive T-cell therapies (28), targeted therapies (29), and convection-enhanced delivery (15) are still in the experimental phase.

In patients with brain metastases, therapeutic management is very heterogeneous and depends on many factors, such as the type of primary cancer, the number and size of brain metastases, and the patient's performance status (Figure 1). These factors vary from one patient to another and require individually tailored management (16, 30, 31) guided by the patient's prognosis (16, 32-35). In patients with a good performance status, initial therapy is based on the number and size of brain lesions. When deemed feasible and expected to prolong survival, resection is an option for patients with a limited number of metastatic brain lesions (up to 3). Resection should also be considered for lesions ≥3 cm in size, regardless of symptoms, and in patients with radioresistant primary tumors (e.g., melanoma or renal carcinoma). After resection, adjunctive radiotherapy of the surgical cavity – using stereotactic radiotherapy/-surgery (SRT/SRS) or whole brain radiotherapy (WBRT) – should be implemented to improve local tumor control and minimize local recurrence, with WBRT entailing a greater risk of neurocognitive decline (16, 36-39). SRS is the first-line treatment option in patients with inoperable lesions and lesions up to 3.5 cm in size (16). In patients with more than three brain metastases, various additional factors need to be considered besides the number of lesions in deciding about the radiotherapeutic regimen (SRS, WBRT, or combined) (16). The following section focuses on radiosurgery as it is the topic of this study.

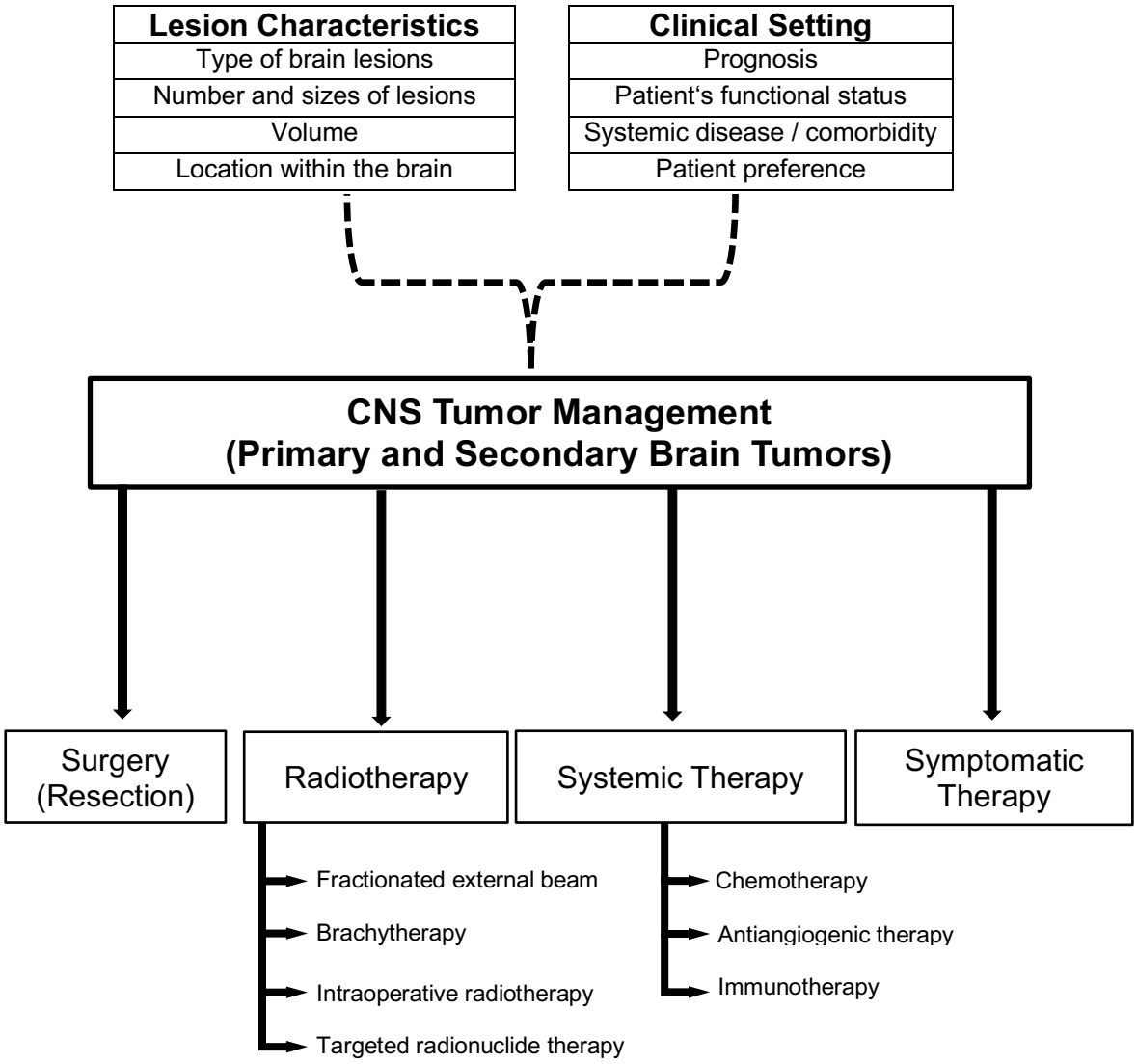

Figure 1. Overview of treatment options in patients with CNS tumors

1.2. Radiosurgery and CyberKnife®

Radiotherapy uses high doses of ionizing radiation to eliminate both benign and malignant tumors (40). It enables treatment of surgically inaccessible intracranial lesions with great patient comfort. General anesthesia is typically not necessary, and patients are not confined to bed after treatment.

Radiotherapy, in general, is governed by the four Rs of radiobiology or fractionation: repair, redistribution, reoxygenation, and repopulation (41). Fractionated dose delivery in radiotherapy takes advantage of the fact that, unlike healthy cells, cancer cells lack the molecular mechanisms to optimally repair DNA damage and stay radioresistant after radiation. In fractionated radiation therapy, the total target dose is not applied in a single session but is divided into multiple smaller doses delivered at different time intervals, thus allowing normal cells to repair DNA damage while attacking cancer cells with a high cumulative dose (42, 43). Fractionated radiotherapy is used for the primary, adjuvant, and palliative treatment of both primary and secondary brain tumors and cancer in other body regions. Brain lesions are typically radiated at 1.8 to 2 Gy per session over several weeks up to a cumulative dose of 30 to 60 Gy (44, 45).

The term ‘radiosurgery’ was coined by neurosurgeon Lars Leksell in 1951 (46) for a neurosurgical technique that uses needles and probes to irradiate a tumor rather than opening the skull to remove it. During the procedure, rigid fixation of the patient's head ensures precise irradiation of the target area (46, 47). Further development introduced the frameless dose-delivery system and replaced the need for needles by using radiation beams, making stereotactic radiosurgery (SRS) a totally noninvasive treatment method (45, 48). Unlike conventional radiation therapy, SRS is typically performed in a single session with application of a high dose of around 11 Gy to 24 Gy, traditionally using a convergence of nonparallel radiation beams (5). The SRS technique achieves a steep dose gradient between the tumor and surrounding tissue, thus minimizing damage to healthy structures. Unlike fractionated radiotherapy, SRS delivers a single high radiation dose that causes irreparable cellular damage and thus can be used in the treatment of otherwise typically radioresistant tumor (5, 45). In fractionated SRS, the total dose is usually divided into fewer fractions (hypofractionation) compared with conventional radiotherapy schedules (44, 45).

Several SRS systems that use different dose-delivery systems are commercially available, among them Leksell Gamma Knife (Elekta, Stockholm, Sweden), Novalis (BrainLAB, Feldkirchen, Germany), and CyberKnife (Accuray, Sunnyvale, CA, USA) (49). Gamma Knife uses a frame-mounted system with multiple isocenters from 192 individual fixed cobalt-60 sources that create numerous converging collimated beams of different sizes; the Novalis system uses linear accelerator-based photon beam production and a multileaf collimator as well as multiple non-coplanar arcs of beams for intensity-modulated radiotherapy; and CyberKnife uses a frameless robot-controlled 6-megavolt linear accelerator with nonisocentric cone beams and 6 degrees of freedom combined with real-time image-to-image correlation, providing submillimeter precision (49, 50).

1.2.1. CyberKnife® Robotic Radiosurgery System

The CyberKnife® Robotic Radiosurgery System is manufactured by Accuray, Inc. (Sunnyvale, California, USA) and was developed by the team of Dr. John Adler, Jr. at Stanford University and Accuray, Inc (51, 52). This system can robotically and actively track, detect, and correct patient movement, thus ensuring frameless real-time image-guided stereotactic irradiation (53, 54). Its main component is a 6-megavolt linear accelerator with a weight of approximately 120 kg mounted on a robotic arm. In addition, the system includes a robotic treatment bed, and two ceiling-mounted diagnostic x-ray cameras with corresponding flat panel silicon detectors on either side of the patient for real-time imaging. The robotic arm and treatment couch each have a total of six degrees of mobility and can actively correct rotational and/or translational offsets during radiation delivery for high accuracy (49, 50, 52). With these features, CyberKnife radiosurgery can be performed without rigid cranial fixation while at the same time improving patient comfort. Compared with other radiosurgery systems that use forward planning and isocentric radiation delivery, CyberKnife uses an inverse planning algorithm to accomplish the steepest dose gradients between the target and surrounding critical structures and healthy brain tissue and nonisocentric beam delivery for homogeneous dose application, which is of particular advantage when irregularly shaped target lesions are treated (49, 55).

1.2.2. Follow-up after Radiosurgery

Response Assessment in Neuro-Oncology (RANO) guidelines are used for monitoring the treatment response of both primary and secondary brain tumors in a standardized manner (56-58). After radiotherapy for brain tumors, patients require regular imaging for the monitoring of treatment outcome and early identification of recurrent tumor. Contrast-enhanced MRI is the standard imaging tool in brain tumor follow-up programs, allowing quantification of tumor volumes for comparison with findings before treatment (5). However, MRI is known to have limited accuracy in differentiating radiation injury/radionecrosis from recurrent tumor (19, 59). In patients with inconclusive MRI findings, PET with radiolabeled amino acid as tracer can help overcome this common problem in the clinical setting (Section 1.3).

1.2.3. Postradiation Effects and Radiation Necrosis

As with all medical procedures, radiotherapy of brain tumors comes with possible complications. They are grouped into acute, early delayed or subacute, and late delayed radiation effects: acute reactions occur during or shortly after exposure to ionizing radiation, subacute effects within a few weeks to several months, and late effects from several months to years after exposure (60). Acute radiation effects include emesis, dizziness, seizures, and headaches, typically caused by increased intracranial pressure. They tend to be mild to moderate and self-limiting or can be relieved with corticosteroids (60-62). Other symptoms include fatigue along with loss of appetite, neurological symptoms, orbital pain, radiation dermatitis, and alopecia (61, 63, 64). Early delayed or subacute effects can present as somnolence, fatigue or pseudoprogression and are also generally reversible and manageable with corticosteroids (60). Late delayed radiation effects, however, are typically irreversible, sometimes progressive, and may even be fatal (60). They include cognition impairment, leukoencephalopathy, radionecrosis, and other radiation-induced CNS toxicity such as telangiectasia or parenchymal brain pathologies (gray/white matter) (60, 62).

Published data on the frequency of radionecrosis after SRS are heterogeneous. Approximately 5 – 25% of the patients are at risk of developing radionecrosis within the first 6 months after SRS (19, 65). In a small study published in 2019, Donovan et al. found a higher radionecrosis rate in the case of multiple brain metastases treated with CK-RS - in 16 out of 22 patients (73%) and in 21 of 62 lesions (34%) - compared to published

results for SRS treatment despite comparable tumor control (66). The risk of radionecrosis after postoperative SRS (9 - 17.5%) is also higher than after postoperative WBRT (2.6%) (16, 67, 68). The overall 1-year cumulative incidence of both reversible and irreversible complications after initial SRS of brain metastases is about 13-14% and is dependent on numerous factors including size, volume and localization within the brain, the SRS technique used, the primary tumor, and the dose-volume ratio (19, 69, 70). Thus, it is of major interest to reliably diagnose radionecrosis and differentiate it from recurrent tumor in clinical routine.

1.3. PET Imaging in Neuro-Oncology - Diagnosing Postradiation Changes

This section presents a general outline of the role of positron emission tomography (PET) imaging in neuro-oncology with a focus on the diagnosis of cerebral postradiation changes in order to explain the rationale for investigating ^{18}F-FET-PET in this study. However, it is beyond the scope of this dissertation to detail the complete range of nuclear medicine modalities in neuro-oncology.

1.3.1. Overview of PET and Its Tracers

PET is a functional imaging modality that allows in vivo assessment of body functions by depicting normal and abnormal metabolic activity following injection of a radioactive drug known as radiotracer. PET tracers are certain short-lived positron-emitting isotopes that are administered at extremely low concentrations (micro- to nanomolar). Cancer cells have a higher metabolic activity than normal cells and appear bright on PET scans. While, due to its better spatial resolution and wide availability, MRI remains the first-line imaging modality, particularly for the initial diagnosis of brain tumors, PET imaging plays an increasingly important role in neuro-oncology because the use of various radiotracers allows imaging of radiotracer-specific metabolic processes in the body (71).

Specific PET tracers are available to measure specific metabolic pathways (59, 72). The standard PET tracer used in clinical oncology is the radiolabeled glucose analogue ^{18}F-2-fluoro-2-deoxy-D-glucose (^{18}F-FDG), which exploits the fact that many cancers have increased glucose metabolism (73). ^{18}F-FDG, however, has several drawbacks in neuro-oncological imaging. Firstly, intracranial tumors have lower contrast on ^{18}F-FDG PET scans than tumors elsewhere in the body because of higher tracer uptake by normal brain parenchyma due to physiologically higher glucose metabolism compared with other body tissues. Secondly, higher tracer uptake also occurs in inflammatory processes, which renders ^{18}F-FDG unspecific (19, 74, 75). Thirdly, ^{18}F-FDG uptake has been shown to correlate with the tumor grade; as a result, some brain tumors such as low-grade gliomas are ^{18}F-FDG-negative and may be missed by PET (74, 76, 77).

To overcome these drawbacks, radiolabeled amino acid tracers were developed. Certain amino acids require specific transporters, making them more specific than the widely

metabolized glucose. Many radiolabeled amino acids have been explored for tumor imaging, and some of them have been evaluated more extensively in human studies. The latter include O-(2-[^{18}F]-fluoroethyl)-l-tyrosine (^{18}F-FET), 6-^{18}F-fluoro-3,4-dihydoxy-Lphenylalanine (FDOPA), 3-^{123}I-iodo-a-methyl tyrosine (^{123}I-IMT), 3-^{18}F-fluoro-a-methyltyrosine (FMT), ^{11}C labeled L-methionine (^{11}C-MET), and cycloleucine analog ^{18}F-FACBC (59, 78).

1.3.2. ^{18}F-FET-PET/CT in Neuro-Oncology

In general, PET is used as an add-on examination to help characterize a suspicious brain lesion in patients with inconclusive MRI findings. ^{11}C-MET and ^{18}F-FET are among the most extensively investigated and most widely used amino acid tracers for brain tumor imaging (59, 79-82). All amino acids could theoretically be radiolabeled with ^{11}C; however, its short half-life of 20 minutes (59, 74) limits its use in institutions that lack cyclotron units. No such drawback exists for ^{18}F, which has a half-life of 110 minutes. ^{18}F-FET is a substrate of L-amino acid transporters (LATs), which are abundant in brain tumors, hence ^{18}F-FET can cross the intact blood-brain barrier, rendering its uptake independent of the status of the blood-brain barrier (83-85). Other advantages are that ^{18}F-FET has lower uptake in healthy brain tissue than FDG and that it is metabolically more stable than ^{11}C-MET and F-DOPA because it is not incorporated into metabolic pathways and consequently has low retention in healthy brain tissue (59, 79, 86).

Since its introduction in 1999 (87), ^{18}F-FET has shown promising results in many neuro-oncological applications ranging from initial diagnostic workup to glioma grading and posttherapeutic monitoring including response assessment and differentiation of radionecrosis from recurrent malignancy (19, 88-92). For instance, Galldiks et al. (2015) showed that ^{18}F-FET-PET had a higher diagnostic accuracy of 93% compared to conventional MRI (85%) in diagnosing recurrent glioma (90). ^{18}F-FET-PET imaging can be performed statically or dynamically. While a static PET scan captures uptake at a single point in time, dynamic PET acquires imaging data on ^{18}F-FET tracer uptake over time, typically for 30 to 40 minutes, thus providing additional information on tumor biology not available from conventional MRI. Quantitative dynamic data are used to generate a time-activity curve (TAC). Distinct TAC patterns have been identified and associated with

different types of brain lesions. Several studies investigating the performance of dynamic ^{18}F-FET-PET/CT in differentiating glioma from radionecrosis report sensitivities of 83-100% and specificities of 78-100% (93-96). For the differentiation of brain metastasis from radionecrosis, investigators report 69-95% sensitivity and 83-93% specificity (88, 89, 97, 98). In a study comparing static and dynamic FET-PET, Galldiks et al. (2012) showed diagnostic accuracy in differentiating recurrent brain metastasis from radionecrosis to increase from 83% with use of a single static parameter (TBR_{mean}) to 92% using a single dynamic parameter (TAC).

1.4. Hypothesis and Objective

It is very challenging to differentiate between radionecrosis and recurrent brain tumor in patients who have undergone radiotherapy. Dynamic ^{18}F-FET-PET/CT is a widely known second-line examination when MRI findings are inconclusive. However, its role in brain lesions treated with CyberKnife – a frameless, high-dose, image-guided robotic radiosurgery technique - has not been sufficiently analyzed yet. Because the acquisition of dynamic ^{18}F-FET-PET parameters is resource-intensive, the benefit of this modality should be clearly established to justify its use. We hypothesize that dynamic parameters derived from ^{18}F-FET-PET/CT are valuable in differentiating radionecrosis from recurrent tumor after CK-RS, as suggested by promising initial results discussed in the preceding section. This single-center study explores and analyzes the clinical value of dynamic ^{18}F-FET-PET/CT in differentiating unclear brain lesions in a patient population with primary and secondary brain tumors after treatment with CyberKnife radiosurgery.

2. Methods

2.1. Study Design and Patient Population

This study retrospectively investigated diagnostic accuracy in the follow-up of patients with primary or secondary brain tumors treated at the CyberKnife Center of Charité – Universitätsmedizin Berlin and was approved by the local ethics committee (Ref EA4/222/17). The study was designed in accordance with the Standards for Reporting of Diagnostic Accuracy Studies (STARD) guidelines (99). Candidates initially screened for inclusion were patients with suspicious brain lesions (tumor recurrence or radionecrosis) on cranial magnetic resonance imaging (cMRI) who subsequently underwent dynamic ^{18}F-FET-PET/CT (index test) after radiosurgery treatment at the Charité CyberKnife Center from 2011 through 2017 (1). A flowchart of routine follow-up care after CyberKnife radiosurgery (CK-RS) in our hospital is presented in Figure 2. The final study population consisted of patients who underwent dynamic ^{18}F-FET-PET/CT following a diagnosis of suspected recurrence with the differential diagnosis of radionecrosis on routine follow-up cMRI (1).

Patients were included regardless of primary tumor site and number of brain lesions. In patients with multiple lesions, only CyberKnife-treated lesions that were suspicious on follow-up cMRI and led to PET referral were analyzed quantitatively. Lesions that were invisible/inactive in ^{18}F-FET-PET/CT were only qualitatively analyzed. Quantitative analysis was performed for all (primary and secondary) brain lesions taken together (TOTAL) and for the subset of metastatic brain lesions (METS) (1).

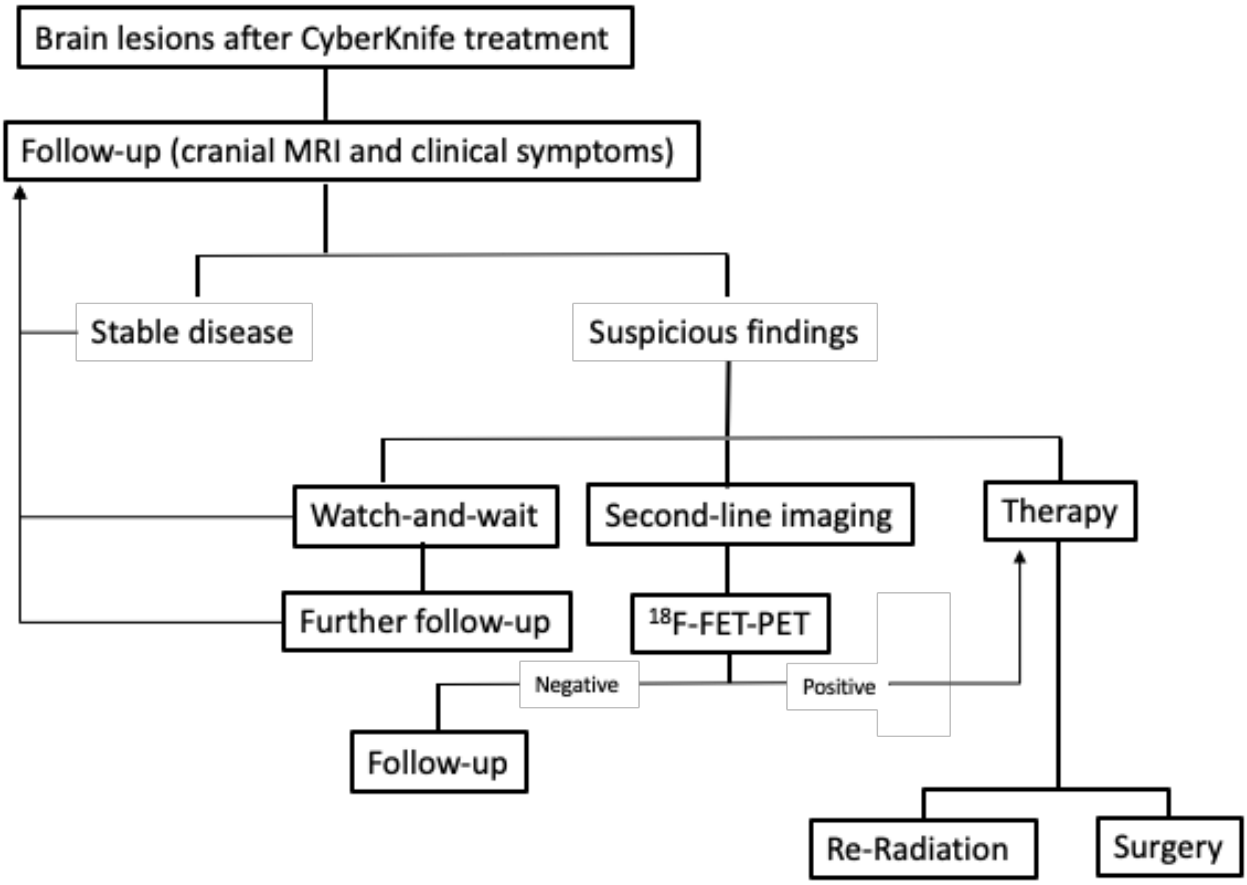

Figure 2. Simplified routine clinical management of patients following CyberKnife radiosurgery of primary and secondary brain tumors

In patients with suspicious findings at follow-up cMRI, clinicians decide between one of three options: further surveillance, additional imaging to clarify the diagnosis, or therapy by repeat radiation or surgery.

2.2. CyberKnife® Treatment

The main principles of routine clinical radiosurgery treatment at Charité CyberKnife Center have been reported before (1, 49, 55, 100). Treatment is generally performed in an outpatient setting. In the study patients, radiation planning was based on thin-sliced CT (0.75 mm) and thin-sliced MRI scans (1 mm, T1-weighted MP-RAGE). These CT and MRI images were fused using Multiplan version 4.5 (Accuray Inc., Sunnyvale, CA) (55). A custom soft mask was fitted for each patient.

Individual treatment planning including dose prescription, determination of isodose lines, and fractionation scheme was performed by a radio-oncologist, a neurosurgeon, and a radiation physicist. The prescribed radiation dose depends on many factors including tumor type, size, total lesion volume, location, and previous irradiation. Technical planning included setting up collimators, reducing dose in areas at risk, defining dose constraints, as well as maximizing dose resolution to evaluate distant scattering of radiation (55).

Before the treatment session, patients were positioned with the aid of in-room lasers. During irradiation, the 6-dimensional skull tracking of the CyberKnife image guidance system was used: real-time images were acquired and compared with the reference CT scan at defined intervals to improve precision. Based on this, therapists get recommendations for possible adjustments for each beam site, allowing precision correction up to 0.1 mm in translations and 0.1° in rotations (100, 101).

Figure 3. CyberKnife system at Charité CyberKnife Center

Photograph courtesy and copyright of Charité Cyberknife Center (102)

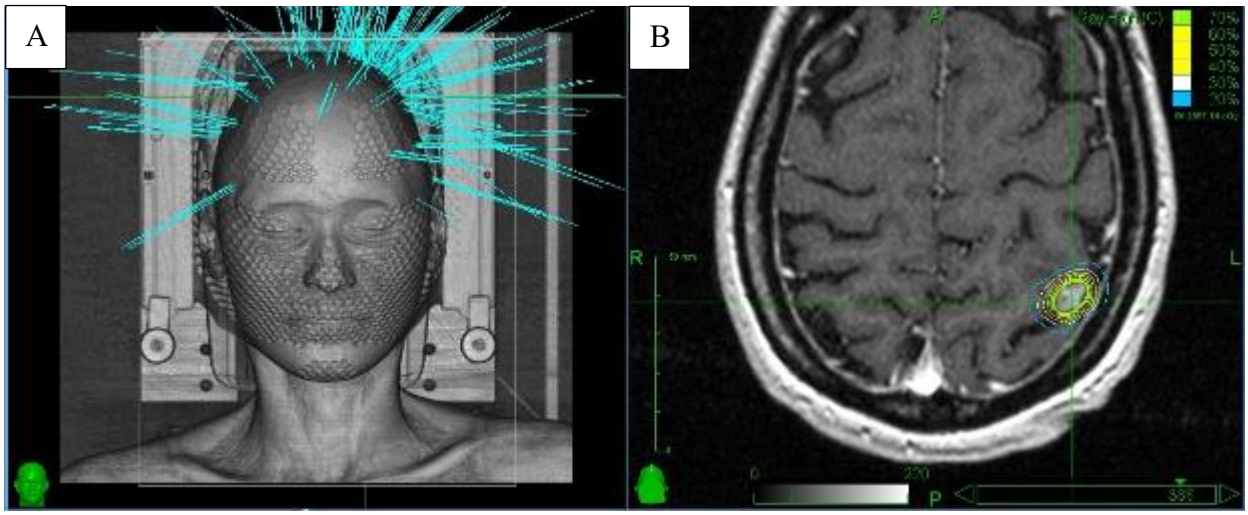

Figure 4. Example illustrating CyberKnife radiation planning

(A) Three-dimensional reconstruction of beam directions (blue lines). (B) Axial view of a left parietal lesion with multiple dose prescription contours; sagittal and coronal views are not shown. Anonymized images from the Charité Cyberknife Center database.

2.3. MRI and ^{18}F-FET-PET/CT Protocols

2.3.1. Magnetic Resonance Imaging

After CK-RS, all patients included in this retrospective analysis underwent regular follow-up using contrast-enhanced cMRI. Many follow-up cMRI examinations were performed in 1.0-1.5 Tesla scanners at outside facilities (1). The study patients who underwent cMRI at Charité University Hospital were examined on MRI scanners with field strengths ranging from 1.5 to 3.0 Tesla. The standard cMRI protocol uses head coil and includes T1- and T2-weighted pulse sequences, diffusion-weighted imaging, and postcontrast T1-weighted 1.0 mm thin-sliced 3-dimensional isovoxel gradient echo imaging after intravenous administration of gadobutrol (Gadovist®, Bayer, 1 mmol/ml) or gadoterate meglumine (Dotarem®, Guerbet, 0.5 mmol/ml) at a dosage of 0.1 mmol/kg of body weight. The postcontrast images were used for multiplanar reconstruction (1).

2.3.2. ^{18}F-FET-PET/CT

^{18}F-FET-PET/CT was performed as described before (1). Briefly, patients were instructed to fast or to be on a protein-low diet for at least 4 hours, to drink approximately 1 liter of water and to empty the bladder prior to the PET/CT examination. Before PET/CT acquisition, the patient's head was positioned and fixated. Imaging data were acquired in the 3-dimensional mode with a Gemini TF 16" (Philips Medical Systems) with the Astonish TF-Upgrade. The 40-min emission scan was started directly after intravenous administration of 150 - 200 MBq ^{18}F-FET. The data were reconstructed using an algorithm with a 128 × 128 matrix size in a single bed position with 16 cm axial field of view (FOV), followed by manual reconstruction using the filter "normal" with 20 dynamic frames in 6 x 20 sec, 8 x 1 min, and 6 x 5 min. For attenuation correction, a low-dose CT scan of the entire head was acquired with 5 mm slice thickness, 30 mAs tube current, 120 kV tube voltage, 0.5 s gantry rotation time, and 512 matrix size (1).

As described in Lim et al. (1), a nuclear medicine physician with more than 15 years of experience in the field semiautomatically placed a region of interest (ROI) in each suspicious lesion and normal brain tissue using a 40% isocontour threshold and determined static and dynamic PET parameters as follows: tissue ^{18}F-FET uptake was expressed as standardized uptake value (SUV), calculated as tissue radioactivity divided

by injected radioactivity per gram of body weight. The maximum SUV (SUV_{max}) of a suspicious lesion was divided by the SUV_{max} in the normal brain ROI to generate the tumor-to-background ratio (TBR). Time to peak (TTP) – which is the time needed from the start of dynamic acquisition until SUV_{max} is reached in the lesion – was measured. A time-activity curve (TAC) was generated, and the patterns were analyzed and interpreted based on three generally accepted TAC patterns first described for glioma grading (89, 92, 93, 98). The three TAC patterns are: TAC I for a slowly and continuously ascending curve indicating the metabolism of non-tumorous lesions, TAC II for an ascending curve followed by a plateau, and TAC III for a descending curve, with both TAC II and III indicating tumorous lesions with higher metabolism. These patterns have been shown to allow differentiation of radionecrosis from recurrent tumor (88-93).

2.4. Data Analysis and Statistics

Each lesion was treated as an individual data point. Whenever available, histopathology reports were used as reference diagnoses. However, in clinical routine and particularly in neurosurgery, histological verification is not always available. In such cases, best supporting evidence based on follow-up imaging and clinical data was used as reference diagnosis, as previously done in other studies (88, 89, 98, 103). Briefly, tumor recurrence was assumed when the contrast-enhanced T1-weighted sequence of follow-up cMRI showed a more than 25% increase in size of an abnormality in a previously treated area according to MacDonald's criteria (104) and / or there were new or worsening neurological deficits associated with the treated area during follow-up. Radiation necrosis was assumed when there was a size decrease in follow-up imaging and neurological deficits remained constant or improved over time. This retrospective evaluation was performed by a neurosurgeon subspecializing in stereotactic surgery with more than 10 years of experience and a nuclear medicine clinician with more than 15 years of experience (1).

As described in Section 2.1, quantitative analysis was performed for all brain lesions (TOTAL) and metastases only (METS). The PET parameters determined in the study population were analyzed to identify possible cut-off values in comparison to published works.

Normal distribution of ^{18}F-FET-PET parameters was tested using the Shapiro-Wilk test. The Mann-Whitney U-test was used to compare groups of not normally distributed samples. The Kruskal-Wallis test was applied to analyze significance of differences in TTP distribution among the three TAC patterns. A post-hoc test (Dunn-Bonferroni test) was employed to determine the validity of significant differences in the pairwise comparison of TAC patterns. The diagnostic accuracy of the index test was analyzed (sensitivity, specificity, accuracy, likelihood ratio, pre- and post-test probability). Regarding pre- and post-test probability, to our knowledge, no exact prevalence data for radionecrosis/recurrence after CyberKnife treatment have been reported so far, therefore pre-test probability was derived from cross-tabulation between MRI findings and the clinical reference diagnosis. Diagnostic probabilities were calculated for different combinations of PET parameters. Improvement of diagnostic probability relative to the pre-PET situation was defined as the difference between pre- and post-test probabilities.

Confidence intervals were used to provide for estimates in accordance with statistical literature (105, 106).

Collection and analysis of data were performed using Microsoft Excel and IBM® SPSS® Statistics Version 24. Data analysis was planned following consultation with iBike (Institute of Biometry and Clinical Epidemiology) of Charité - Universitätsmedizin Berlin.

3. Results

3.1. Study Population and Characteristics

A total of 29 patients with suspected recurrence or radionecrosis after CK-RS were initially screened for inclusion (Figure 5). Patients without dynamic ^{18}F-FET-PET/CT during follow-up were excluded. Another two patients with lesions not showing uptake in dynamic ^{18}F-FET-PET were analyzed qualitatively, leaving 14 patients eligible for quantitative analysis.

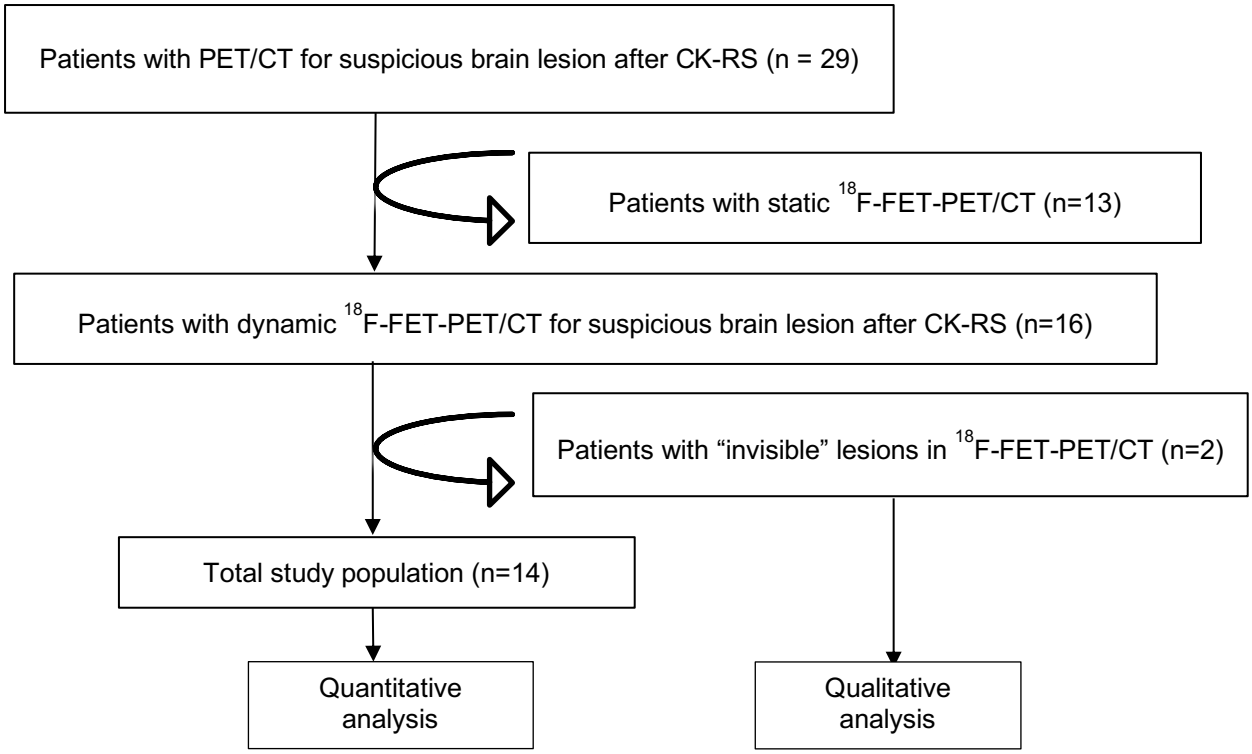

Figure 5. Flowchart of patient recruitment

CK-RS = CyberKnife – stereotactic radiosurgery.

Adapted from the original publication of Lim et. al. (1)

The 14 patients included in the quantitative analysis (2 males, 12 females) had a median age of 52 years (range 16-79 years). Three patients had a single brain lesion (Σ n = 3). Nine patients had two brain lesions (Σ n = 18). One patient had three brain lesions (Σ n = 3). One patient had four brain lesions (Σ n = 4). Histological confirmation was available for 7 of the 28 brain lesions (25%) in five patients. Six patients (43%) with a total of 13 lesions (46%) underwent WBRT before CK-RS treatment (Table 2).

Table 2. Patient demographics and lesion distribution

Age	median 52 years; range 16-79 years	
Sex	2 (14%) males / 12 (86%) females	
Number of Brain Lesion(s) per Patient	**Number of Patients (%)**	**Number of Lesions (%)**
1	3 (21.4)	3 (10.7)
2	9 (64.3)	18 (64.3)
3	1 (7.1)	3 (10.7)
4	1 (7.1)	4 (14.3)
Total	14 (100)	28 (100)
Histology available in	5 (36)	7 (25)
WBRT (prior to CK-RS)	6 (43)	13 (46)

Adapted from the original publication of Lim, et. al. (1)

A total of 28 lesions in 14 patients were included in this retrospective analysis: 23 metastatic brain tumors in 12 patients and 5 primary brain tumor lesions in two patients (Table 3). The primary brain tumors were an ependymoma and a PTPR (papillary tumor of penial region). Primaries of secondary brain tumors included breast cancer in 9 patients, non-small-cell lung cancer in 2 patients, and malignant melanoma in 1 patient.

Table 3. Distribution of primary tumors in the study population

Diagnosis		No of Patients (in %)	No of Lesions (in %)
Primary Brain Tumor	**Ependymoma**	1 (7.14)	3 (10.71)
	PTPR	1 (7.14)	2 (7.14)
Brain Metastasis	**Breast cancer**	9 (64.29)	18 (64.29)
	Non-small-cell lung cancer	2 (14.29)	3 (10.71)
	Malignant melanoma	1 (7.14)	2 (7.14)
Total		14 (100)	28 (100)

PTPR = Papillary tumor of the pineal region. Three lesions without tracer uptake in PET (metastasis from breast and lung cancers) are not included in the table. Adapted from the original publication of Lim et al. (1)

CK-RS treatment characteristics were similar in the two groups compared (TOTAL and METS) (Table 4). All CK-RS treatments were unfractionated with a median prescription dose of 19 Gy (range of 13 – 20 Gy for TOTAL and 16 – 20 Gy for METS), median planning and gross tumor volumes of 1.4 to 1.5 cm^3 (range 0.20 – 11 cm^3 for both groups). The median time interval between a patient's last CK-RS treatment and ^{18}F-FET-PET/CT was 10 and 9 months in TOTAL and METS, respectively (range 4 – 35 months for TOTAL and 4 – 23 months for METS). Dynamic ^{18}F-FET-PET/CT was performed in average 15 days (range 7-30 days) after a patient's last MRI examination. For patients who underwent WBRT before CK-RS treatment, the median interval between WBRT and ^{18}F-FET-PET/CT was 28 and 29 months in TOTAL and METS, respectively. Four metastatic lesions (16.7% in TOTAL, 17.4% in METS) in 3 patients were treated twice with CK-RS before dynamic ^{18}F-FET-PET/CT. The median interval between these two CK-RS sessions was 58 weeks (range 27.6-70.90 weeks). Primaries of the four lesions were malignant melanoma, non-small-cell lung cancer, and breast cancer.

Table 4. CyberKnife treatment characteristics

	Mean (SD)		Median		Min-Max	
	TOTAL (n=28)	**METS (n=23)**	**TOTAL (n=28)**	**METS (n=23)**	**TOTAL (n=28)**	**METS (n=23)**
No. Of Fractions	1	1	1	1	n.a.	n.a.
Prescription Dose (Gy)	18.56 (1.9)	19.00 (1.0)	19.00	19.00	13-20	16 - 20
PTV (cm^3)	2.1 (2.6)	2.35 (2.8)	1.45	1.50	0.19 - 11.02	0.20 - 11.02
GTV (cm^3)	2.06 (2.6)	2.35 (2.8)	1.36	1.50	0.19 - 11.02	0.20 - 11.02
Dose min (Gy)	17.58 (1.8)	17.87 (1.2)	17.8	17.90	11.7 - 20	15.51 - 20.00
Dose max (Gy)	26.1 (2.9)	26.76 (1.9)	27.08	27.10	18.1 - 29	21.17 - 28.57
Coverage (%)	98.4 (2.0)	98.3 (2.1)	99.1	99.11	92 - 100	92 - 100
Last CK-RS-to-PET interval (mo.)	12.96 (7.3)	11.46 (5.8)	10.00	9.00	4 - 35	4 - 23
Last MRI-to-PET interval (mo.)	0.55 (0.2)	0.51 (0.3)	0.49	0.49	0.23 - 1.02	0.23 - 1.02
WBRT-to-PET interval (mo.)	25.43 (16.1)	29.25 (8.6)	28.16	29.26	2.3 - 47	16.95 - 40.18
No of CK-RS treatments before FET-PET					**TOTAL (n=28)**	**METS (n=23)**
1					24 (85.7%)	19 (82.6%)
2					4 (16.7%)	4 (17.4%)

Results are presented for all lesions analyzed (TOTAL) and and the subset of metastatic lesions (METS). SD = standard deviation, Gy = Gray, PTV = planning tumor volume, GTV = gross tumor volume, CK-RS = CyberKnife® radiosurgery, PET = positron emission tomography, mo. = months, MRI = magnetic resonance imaging, WBRT = whole brain radiotherapy. Adapted from the original publication of Lim et. al. (1)

The interval between CK-RS and dynamic ^{18}F-FET-PET/CT was shortest (4 months) in patients with brain metastasis from breast cancer (Table 5). The interval between the last CK-RS and dynamic ^{18}F-FET-PET/CT varied the least in malignant melanoma (11 months), while there was a relatively wide range for other primaries. The range was widest for ependymoma with a min-max range of 9-35 months.

Table 5. CyberKnife-to-^{18}F-FET-PET intervals in months by primary tumor

Primary Tumor	No of Patients	No of Lesions	Mean Interval (SD)	Median Interval	Min-Max
Ependymoma	1	3	21.3 (13)	20	9-35
PTPR	1	2	15.5 (9.2)	15.5	9-22
Non-small-cell lung cancer	2	3	15.3 (8)	20	6-20
Breast cancer	9	18	11.1 (5.8)	8.5	4-23
Malignant melanoma	1	2	11 (0.0)	11	11-11

SD = Standard deviation, PTPR = Papillary tumor of the pineal region. Three lesions without tracer uptake in PET (metastasis from breast and lung cancers) are not included in the table.

One patient with non-small-cell lung cancer had one PET-active brain lesion, which was included in quantitative analysis, and one PET-inactive brain lesion, which was excluded from quantitative analysis. Two further patients each had one PET-inactive lesion, amounting to a total of 3 lesions with suspicious MRI findings that appeared inactive in the ^{18}F-FET-PET examination. These three lesions were excluded from quantitative parameter analysis and were only qualitatively analyzed.

3.2. Results of Data Analysis

3.2.1. Static ^{18}F-FET-PET/CT Parameters

Maximum Tumor-to-Background Ratio

In both TOTAL (n = 28) and METS (n = 23), TBR_{max} was normally distributed in the radionecrosis subset and the recurrent tumor subset (Shapiro-Wilk test). TBR_{max} tended to be higher in recurrent tumor than in radionecrosis in both TOTAL and METS (Tables 6 and 7).

Mean Tumor-to-Background Ratio

In both TOTAL and METS, TBR_{mean} was normally distributed in the radionecrosis subset but not normally distributed in the tumor recurrence subset (Shapiro-Wilk test). Similar to TBR_{max}, TBR_{mean} tended to be higher in recurrent tumor than in radionecrosis (Tables 6 and 7).

Table 6. Results for static and dynamic ^{18}F-FET-PET parameters in the whole study population (TOTAL)

TOTAL (n = 28)							
	Tumor (n = 20)*			Radionecrosis (n = 8)*			
	Mean (SD)	95% CI	Median	Mean (SD)	95% CI	Median	p-value**
TBRmax	5.8 (2.6)	(4.6; 7.0)	5.5	4.3 (2.0)	(2.6; 5.9)	3.8	0.15
TBRmean	3.0 (1.4)	(2.4; 3.7)	2.6	2.3 (0.7)	(1.7; 2.9)	2.1	0.12
TTP (min)	9.6 (6.8)	(6.4; 12.8)	7.3	16.7 (14.2)	(4.8; 28.5)	7.3	0.82

*Reference diagnosis.**t-test for TBRmax, Mann-Whitney U-test for TBRmean and TTP. SD = Standard deviation, CI = Confidence interval, TBR = Tumor-to-background ratio, TTP = Time to peak, min = minutes

Table 7. Results for static and dynamic ^{18}F-FET-PET parameters in the metastasis group (METS)

METS (n = 23)							
	Tumor (n = 16)*			Radionecrosis (n = 7)*			
	Mean (SD)	95% CI	Median	Mean (SD)	95% CI	Median	p-value**
TBRmax	5.3 (2.1)	(4.2; 6.5)	5.0	3.8 (1.5)	(2.4; 5.2)	3.5	0.01
TBRmean	2.6 (0.66)	(2.3; 3.0)	2.4	2.1 (0.5)	(1.6; 2.6)	2.0	0.10
TTP (min)	8.3 (3.4)	(6.5; 10.1)	7.3	13.7 (13.1)	(1.6; 25.9)	7.3	0.58

*Reference diagnosis. **t-test for TBRmax, Mann-Whitney U-test for TBRmean and TTP. SD = Standard deviation, CI = Confidence interval, TBR = Tumor-to-background, TTP = Time to peak, min = minutes

A histological diagnosis was available for 7 lesions (6 recurrent tumors and 1 radionecrosis). In this subset, median TBR_{max} was 4.6 for recurrence and 2.3 for radionecrosis. Median TBR_{mean} was 2.8 and 1.9, respectively (Table 8).

Table 8. Results for static and dynamic ^{18}F-FET-PET parameters in 7 lesions with histology

HISTOLOGY (n = 7)				
	Tumor (n = 6)*			Radionecrosis (n = 1)*
	Mean (SD)	95% CI	Median	n/a
TBRmax	5.4 (2.4)	(2.9; 8.0)	4.6	2.3
TBRmean	2.9 (0.6)	(2.2; 3.5)	2.8	1.9
TTP (min)	7.5 (1.6)	(5.8; 9.1)	7.3	35.3

*Histological (reference) diagnosis. p-value is not applicable due to n = 1 in radionecrosis. SD = Standard deviation, CI = Confidence interval, TBR = Tumor-to-background ratio, TTP = Time to peak, min = minutes

ROC analyses were performed to identify possible cut-off values for maximum and mean TBR as diagnostic PET parameters. The best cut-off values were 4.12 for TBR_{max} and 2.13 for TBR_{mean} for both TOTAL and METS. These cut-off values had only 70% sensitivity with 62.5% specificity for TBR_{max} and 75% sensitivity with 62.5% specificity for TBR_{mean} in TOTAL. In METS, these cut-off values had 62.5% sensitivity and 71.4% specificity for TBR_{max} and 68.8% sensitivity with 71.4% specificity for TBR_{mean}. Both parameters had suboptimal to low diagnostic power in TOTAL and METS with an area under the curve (AUC) < 0.75 and p >0.05 (Figure 6).

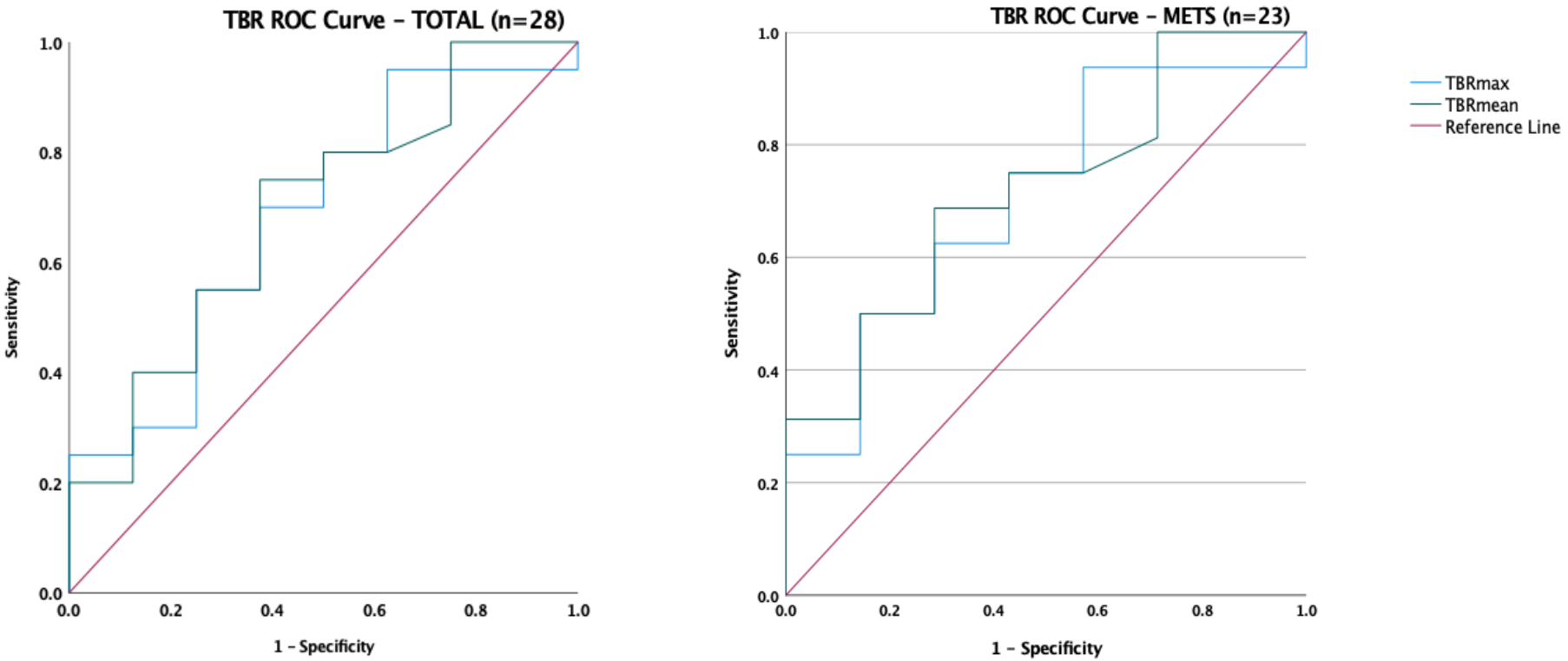

		Cut-Off Value	Sensitivity	Specificity	AUC	95% CI	p-value
TOTAL	**TBRmax**	4.12	70%	62.5%	0.68	0.46 - 0.91	0.14
	TBRmean	2.13	75%	62.5%	0.69	0.47 – 0.91	0.12
METS	**TBRmax**	4.12	62.5%	71.4%	0.71	0.47 – 0.94	0.12
	TBRmean	2.13	68.8%	71.4%	0.72	0.50 – 0.94	0.10

Figure 6. ROC curve of TBR values in TOTAL and METS

The table below the curves lists the best tumor-to-background ratio (TBR) cut-off values derived from the curves with their corresponding diagnostic values, areas under the curve (AUC), 95% confidence intervals (CI), and p-values.

3.2.2. Dynamic ^{18}F-FET-PET/CT Parameters

In dynamic ^{18}F-FET-PET/CT examinations, the time-activity curve (TAC) and time to peak (TTP) reflect tracer uptake over time, providing further information for lesion characterization.

Time to Peak

TTP values were not normally distributed (Shapiro-Wilk test). No difference was found in median TTP values between recurrent tumor and radionecrosis in either TOTAL or METS (median = 7.3). Mean TTP was shorter in recurrent tumor than in radiation necrosis in both TOTAL and METS (Tables 6 and 7).

The six histologically confirmed recurrent tumor lesions had a mean TTP of 7.5 min and a median TTP of 7.3 min, and the one histologically confirmed radiation necrosis had a TTP of 35.3 min (Table 8).

ROC analysis performed to identify possible cut-off values for TTP yielded 25.3 min for both TOTAL (95% sensitivity and 37.5% specificity) and METS (100% sensitivity and 28.6% specificity). AUCs were < 0.55, and p-values were not significant (Figure 7).

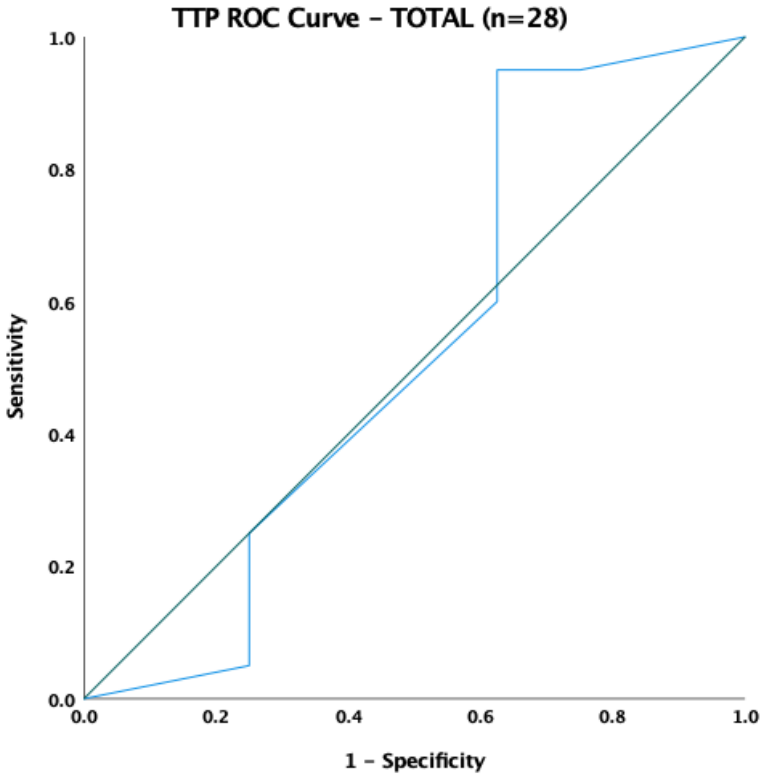

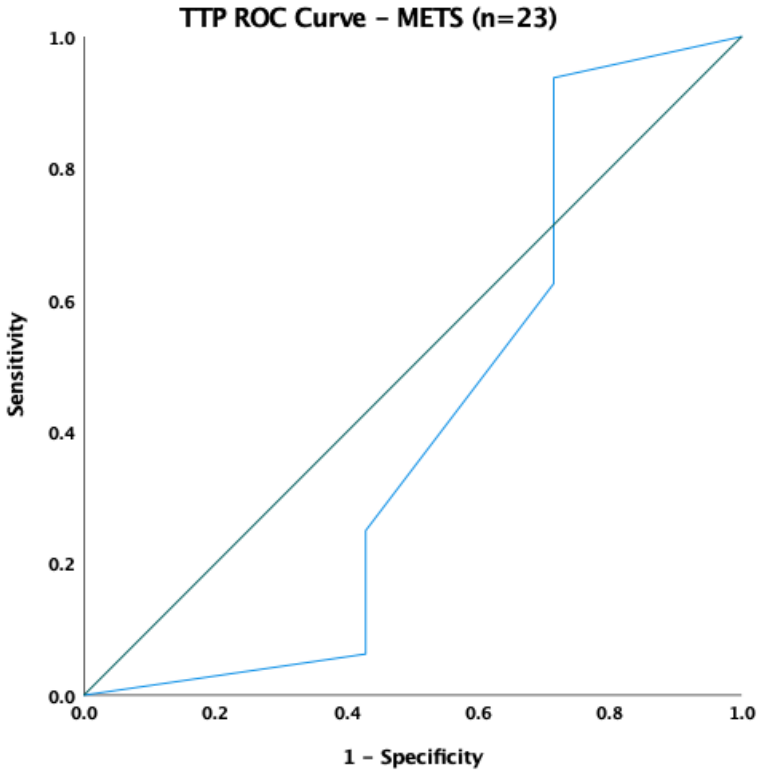

	Cut-Off Value	Sensitivity	Specificity	AUC	95% CI	p-value
TOTAL	25.3 min	95%	37.5%	0.53	0.25 - 0.81	0.82
METS	25.3 min	100%	28.6%	0.42	0.11 – 0.74	0.57

Figure 7. ROC curve of TTP values in TOTAL and METS

The table below the curves lists the best time to peak (TTP) cut-off values derived from the curves with their corresponding diagnostic values, areas under the curve (AUC), 95% confidence intervals (CI), and p-values.

Time-Activity Curve Patterns

Three types of TAC patterns were found in the study population and are illustrated in Figure 8: continuously ascending curve (TAC I), ascending curve followed by a plateau (TAC II), and ascending curve followed by descending curve and long plateau (TAC III).

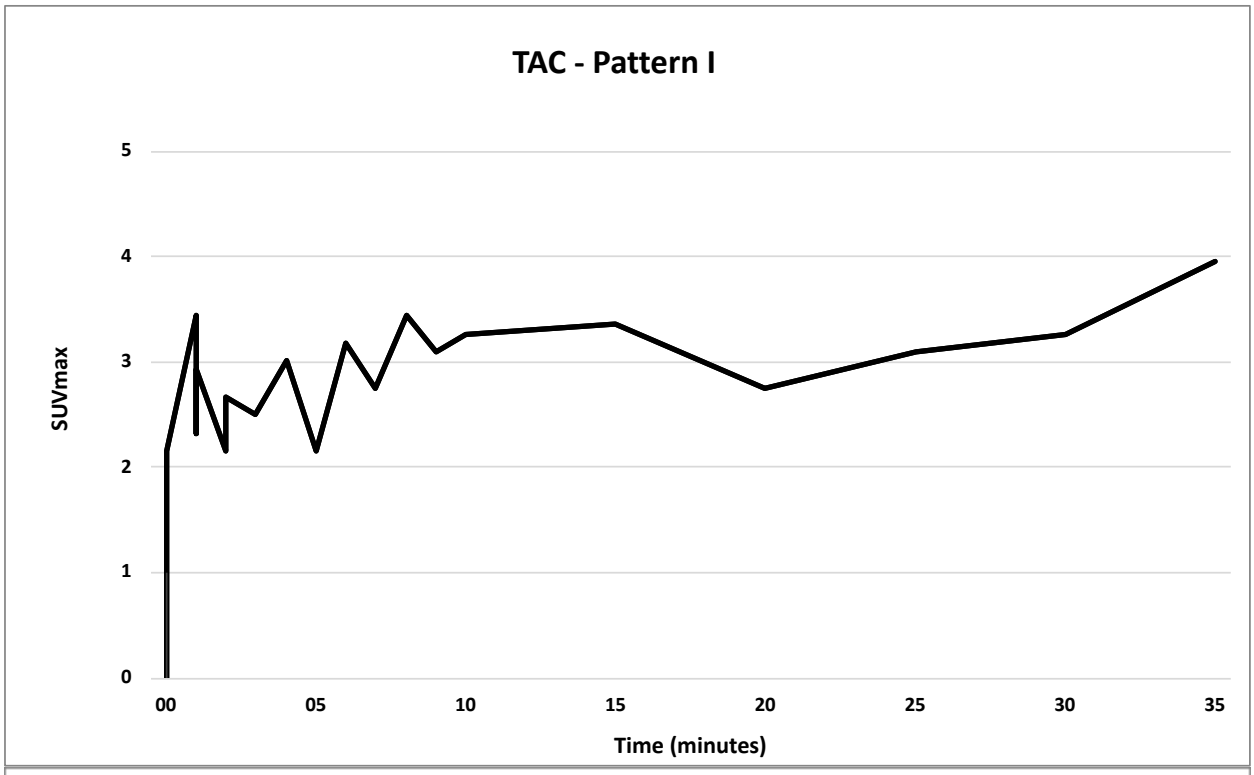

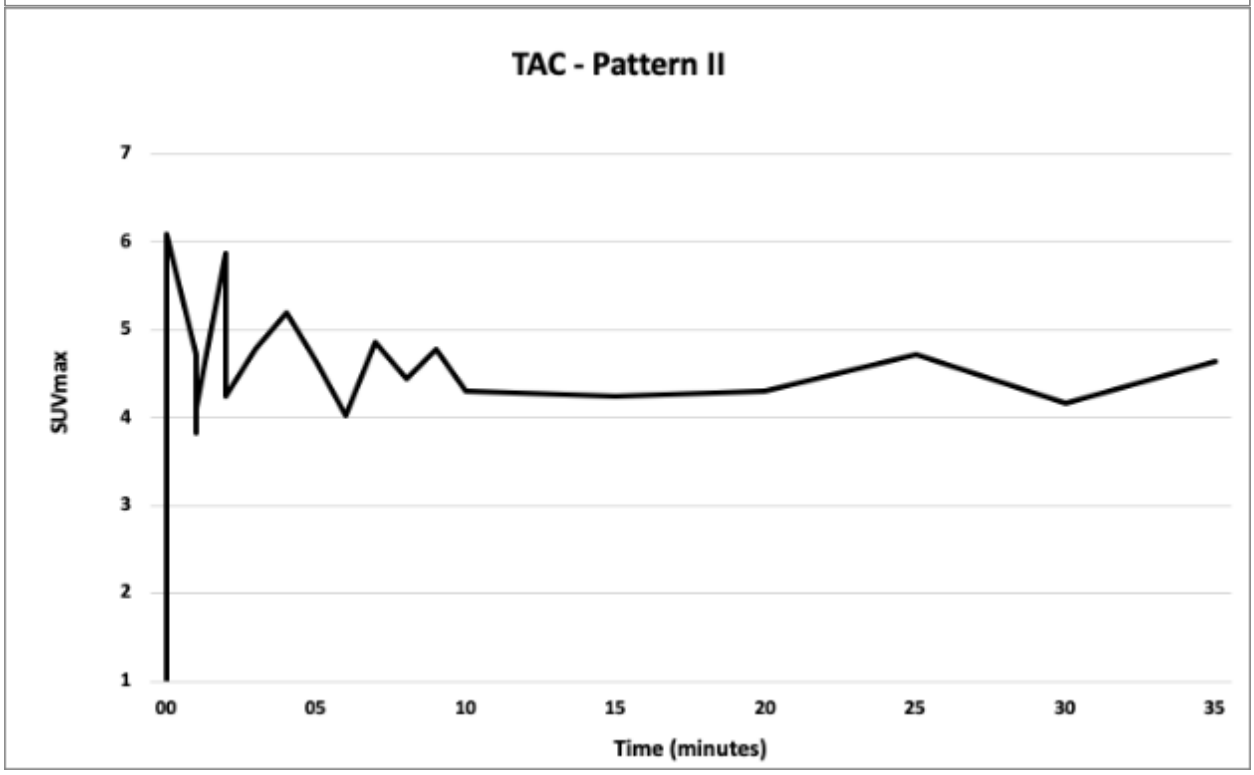

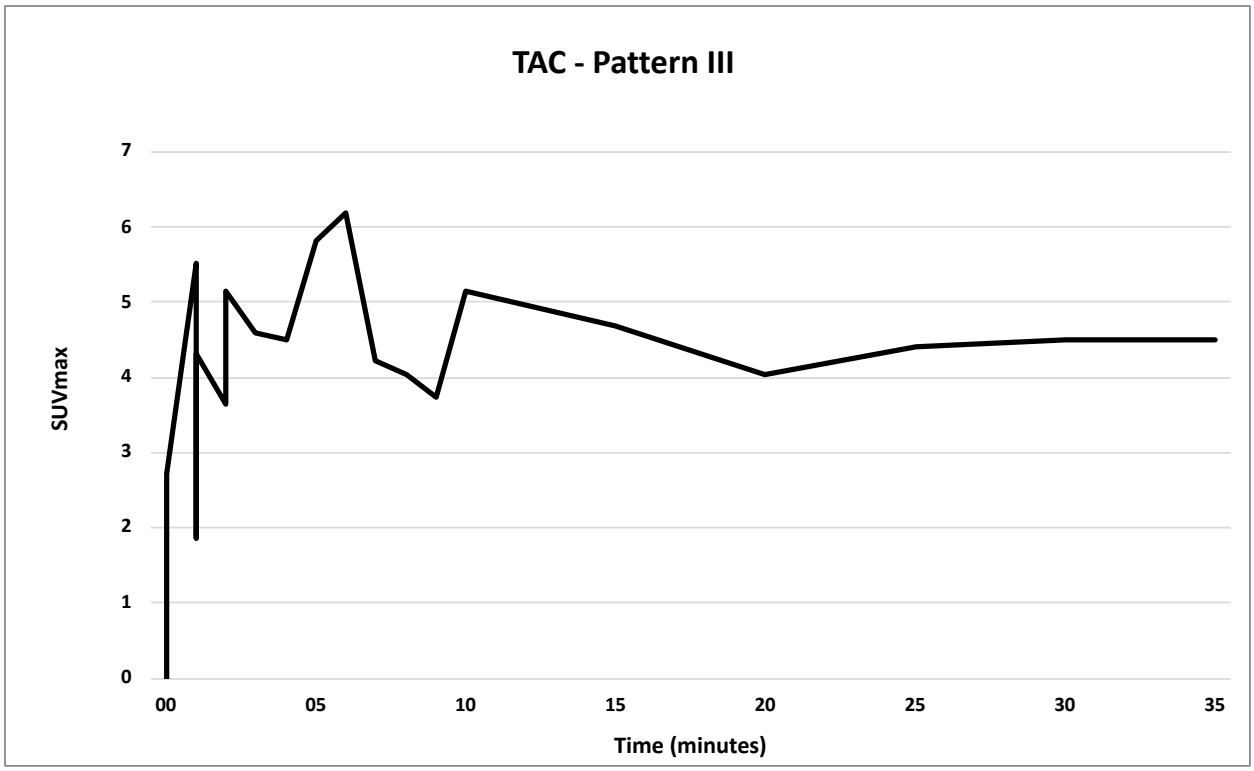

Figure 8. Examples illustrating the three TAC patterns found in the study population

TAC I: continuously ascending curve.
TAC II: steep ascent with slow descent
TAC III: steep ascent followed by small descent and long plateau.

In the TOTAL group of 28 lesions, 5 (18%) had TAC pattern I, 15 (54%) had TAC pattern II, and 8 (29%) lesions had TAC pattern III (Table 9a.). In the METS group of 23 lesions, 4 (17%) had TAC pattern I, 11 (48%) TAC pattern II, and 8 (35%) lesions had TAC pattern III (Table 9b). The six histologically confirmed tumor lesions had TAC pattern II or III, and the one histologically confirmed radionecrosis had TAC I (Table 9c and 10).

Overall, TTP was longer in the radionecrosis group (TAC I) than in the recurrent tumor group (TAC II or III) (Table 9a-c). Mean TTP values of histologically confirmed tumor lesions did not differ much (8 min for TAC II vs. 7 min for TAC III, respectively; Table 9c). There was a significant difference in TTP distribution across the three TAC patterns in the TOTAL group ($p < 0.05$) but not in the METS group ($p > 0.10$). The post-hoc Dunn-Bonferroni test showed that this difference in TOTAL was only between TAC I and TAC III ($p = 0.004$ with a large effect size of 0.88 according to Cohen (107)) with median values of 35.3 min for TAC I vs. 6.8 min for TAC III and mean values of 28.7 min for TAC I vs.

6.8 min for TAC III. Other pairwise comparisons in TOTAL (TAC I vs. TAC II and TAC II vs. TAC III) revealed no significant differences.

Table 9. Distribution of TAC patterns and TTP values

a.

TOTAL (Σ n = 28)				
	n (%)	**TTP Mean (SD)**	**TTP Median**	**Min-Max**
TAC I	5 (18%)	28.7 (12.2)	35.3	7.3-35.3
TAC II	15 (54%)	8.5 (3.5)	7.3	5.3-20.3
TAC III	8 (29%)	6.8 (1.3)	6.8	5.3-9.3

b.

METS (Σ n = 23)				
	n (%)	**TTP Mean (SD)**	**TTP Median**	**Min-Max**
TAC I	4 (17%)	19.6 (15.5)	18.8	5.3-35.3
TAC II	11 (48%)	8.8 (4.0)	7.3	5.3-20.3
TAC III	8 (35%)	6.8 (1.3)	6.8	5.3-9.3

c.

HISTOLOGY (Σ n = 7)				
	n (%)	**TTP Mean (SD)**	**TTP Median**	**Min-Max**
TAC I	1 (14%)		35.3*	
TAC II	3 (43%)	8.0 (1.2)	7.3	7.3-9.3
TAC III	3 (43%)	7.0 (2.1)	6.3	5.3-9.3

* no mean, median or min-max values available due to n = 1.

Adapted from the original publication of Lim et. al. (1)

3.2.3. Diagnostic Accuracy

The ROC analysis results presented in Sections 3.2.1 and 3.2.2 identified no significant cut-offs with high diagnostic power. We therefore used published cut-off values with proven high diagnostic accuracy to assess the diagnostic performance of static and dynamic ^{18}F-FET-PET parameters in our study population. We used the parameter

combination published in Galldiks et al., 2012 (TBR_{mean} > 1.95 combined with TAC II or III and TTP ≤20 minutes as cut-off values for tumor) (89).

In our small study population, ^{18}F-FET-PET/CT correctly diagnosed all 7 lesions for which histological reference diagnoses were available (Table 10).

Table 10. Cross-tabulation between histology reports (n = 7) and ^{18}F-FET-PET/CT findings

		Histology		Total
		Tumor	**Radionecrosis**	
^{18}F-FET-PET/CT	**Tumor**	6	0	6
	Radionecrosis	0	1	1
Total		6	1	7

In the TOTAL group (n = 28), the pre-test probability of correctly differentiating a suspicious lesion was about 71% with pre-test odds = 2.5 (Table 11). In this group, 80% sensitivity, 38% specificity, and 68% accuracy were reached when the static parameter, TBR_{mean}, was used as the only diagnostic parameter, yielding a positive likelihood ratio (LR+) of 1.28 and a negative likelihood ratio (LR-) of 0.53. For the TAC pattern alone, accuracy was 82% with 95% sensitivity, 50% specificity, LR+ = 1.90, and LR- = 0.10. For TTP alone, accuracy was 79% (95% sensitivity, 38% specificity 38%, LR+ = 1.52, LR- = 0.13).

In the METS group (n = 23), pre-test probability was approximately 70% with pre-test odds of 2.3, which is comparable to the TOTAL group (Table 11). TBR_{mean} alone achieved an accuracy of 65% (75% sensitivity, 43% specificity, LR+ = 1.31, LR- = 0.58). TTP alone had 74% accuracy (94% sensitivity, 29% specificity, LR+ of 1.31 and LR- of 0.22. The TAC pattern alone resulted in 87% accuracy (100% sensitivity, 57% specificity, LR+ of 2.33 and LR- of 0.00).

In addition, various combinations of static and dynamic parameters were analyzed (Table 11). In TOTAL, the combination of TBR_{mean} and TAC pattern had 71% accuracy (75% sensitivity, 63% specificity, LR+ of 2, LR- 0.40) and post-test probability of 83%, corresponding to a 12% improvement in diagnostic probability (difference of pre- and

post-test probability). In the METS, the combination of these two parameters achieved 74% accuracy (75% sensitivity, 71% specificity, LR+ 2.63, LR- 0.35) and a post-test probability of 86%, corresponding to a 16% improvement in diagnostic probability. For the combined use of three parameters - TBR_{mean}, TAC pattern, and TTP – similar post-test diagnostic probabilities of 82% and 83% were achieved, corresponding to improvements in diagnostic probability by 11% for TOTAL and 13% for METS (Table 11).

Overall, use of dynamic ^{18}F-FET-PET/CT parameters resulted in better accuracy values (Figure 9). TBR_{mean} alone had 68% and 65% accuracy in TOTAL and METS, respectively. Once dynamic parameters were used, any kind of combination increased accuracy. The highest accuracies of 82% in TOTAL and 87% in METS were achieved using the TAC pattern as the only diagnostic parameter. Combined static and dynamic parameters (TBRmean, TAC, and TTP) resulted in 79% and 83% accuracy in TOTAL and METS, respectively.

Table 11. Diagnostic performance results using single and combined static and dynamic PET parameters for all lesions (TOTAL) and metastatic lesions only (METS)

TOTAL (n = 28)					
			Pre-Test Odds / Probability		2.5 / 71%
	Sensitivity (95% CI)	**Specificity (95% CI)**	**Accuracy (95% CI)**	**LR+ (95% CI)**	**LR- (95% CI)**
TBRmean	80% (56-94)	38% (9-76)	68% (48-84)	1.28 (0.72-2.29)	0.53 (0.15-1.87)
TTP	95% (75-100)	38% (9-76)	79% (59-92)	1.52 (0.88-2.62)	0.13 (0.02-1.10)
TAC	95% (75-100)	50% (16-84)	82% (63-94)	1.90 (0.94-3.83)	0.10 (0.01-0.76)
TBRmean+TAC	75% (51-91)	63% (24-91)	71% (51-87)	2 (0.79-5.07)	0.40 (0.16-1.01)
			Post-Test Odds / Probability		5.0 / 83%
TBRmean+TAC+TTP	90% (68-99)	50% (16-84)	79% (59-92)	1.80 (0.89-3.65)	0.20 (0.05-0.88)
			Post-Test Odds / Probability		4.5 / 82%

METS (n = 23)					
			Pre-Test Odds / Probability		2.3 / 69.6%
	Sensitivity (95% CI)	**Specificity (95% CI)**	**Accuracy (95% CI)**	**LR+ (95% CI)**	**LR- (95% CI)**
TBRmean	75% (48-93)	43% (10-82)	65% (43-84)	1.31 (0.65-2.65)	0.58 (0.17-1.95)
TTP	94% (70-100)	29% (4-71)	74% (52-90)	1.31 (0.81-2.13)	0.22 (0.02-2.03)
TAC	100% (79-100)	57% (18-90)	87% (66-97)	2.33 (0.99-5.49)	0.00 (n.a.)
TBRmean+TAC	75% (48-93)	71% (29-96)	74% (52-90)	2.63 (0.79-8.76)	0.35 (0.13-0.92)
			Post-Test Odds / Probability		6.00 / 86%
TBRmean+TAC+TTP	94% (70-100)	57% (18-90)	83% (61-95)	2.19 (0.92-5.19)	0.11 (0.01-0.81)
			Post-Test Odds / Probability		5.0 / 83%

Adapted from the original publication of Lim et al. (1)

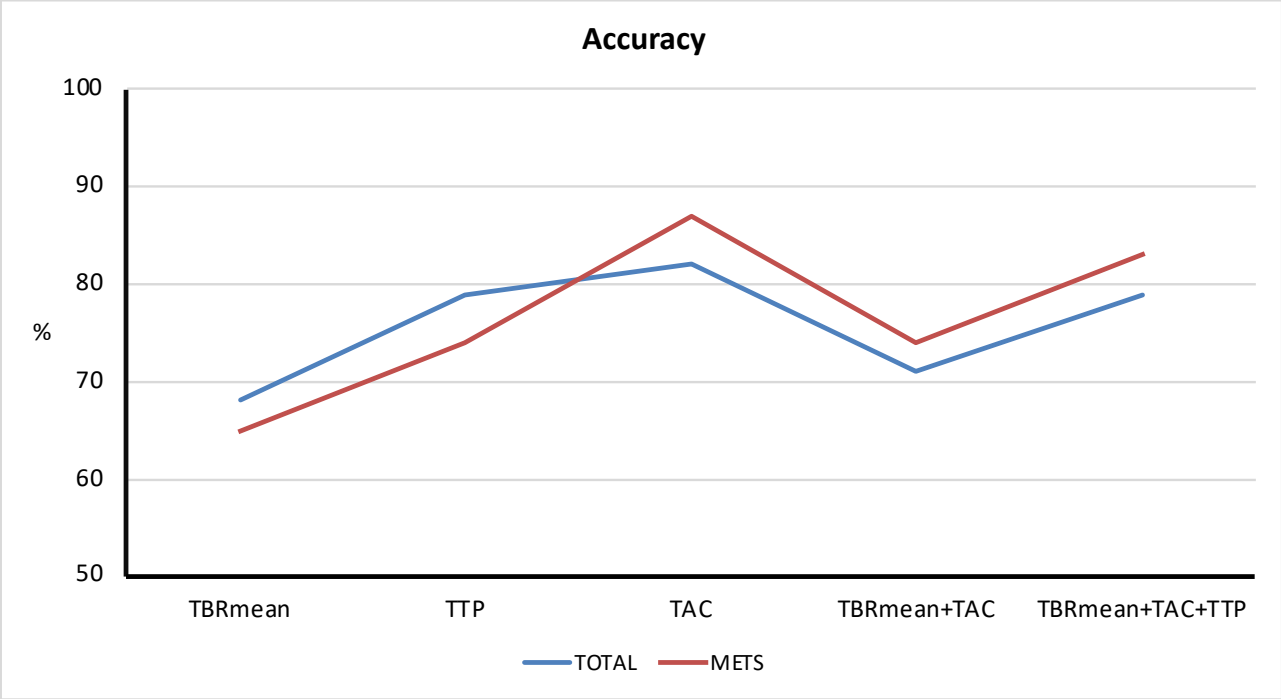

Figure 9. Graphic representation of accuracy values of individual PET parameters and their combinations investigated for all brain lesions (TOTAL) and metastatic brain lesions (METS)

3.2.4. ^{18}F-FET-PET-Negative Lesions

For the three suspicious lesions without tracer uptake in ^{18}F-FET-PET/CT, qualitative analysis was performed. The first case is a glioblastoma, shown in Figure 10, that appeared suspicious in follow-up MRI but was ^{18}F-FET-negative in the subsequent PET examination (Figure 10b). Further follow-up MRI examinations performed after PET showed increasing loss of enhancement of the suspicious area in contrast-enhanced images over time (Figure 10c-f), and the lesion was ultimately assumed to be a radionecrosis. The other two negative lesions, presented in Figures 11 and 12, nicely illustrate the challenges clinicians face in differentiating suspicious lesions. Despite the striking MRI appearance of the lesion (indicated by arrow) in Figure 11a, there was no tracer uptake in ^{18}F-FET-PET (Figure 11b). The case in Figure 12 is of particular interest: in this patient with multiple brain metastases, the two lesions depicted in Figure 12d (dotted arrows) and the posterior right horn lesion in 12j (solid arrow) were treated in the same CK-RS session. However, they differed in terms of ^{18}F-FET tracer uptake: whereas two lesions showed good tracer uptake, thus suggestive of viable tumor (Figure 12e), the other lesion (Figure 12j) was negative in the PET image (Figure 12k). This index case underlines the role of molecular imaging tracers and in vivo tumor characterization in PET

in differentiating viable tumor from radionecrosis in multiple lesions with the same treatment history.

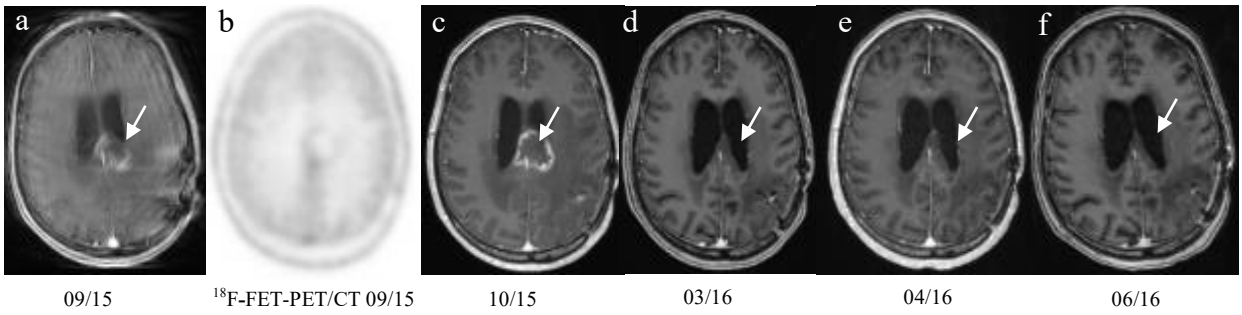

Figure 10. Patient with glioblastoma

Serial contrast-enhanced MR images obtained after CK-RS with PET examination performed after detection of suspicious lesion in MRI: (a) and (c) – (f) are postcontrast T1-weighted MRI images, (b) is a PET image.

CK-RS was performed on the tumor lesion near the corpus callosum/left lateral ventricle (arrow) in July 2015. MRI follow-up in September 2015 shows a suspicious lesion measuring about 2.6 cm (arrow in (a)). The lesion is metabolically inactive in the subsequent ^{18}F-FET-PET examination (b). Repeat follow-up MRI shows less and less pronounced enhancement of the lesion over time, and the lesion is almost undetectable (arrow in (f)) in the last MRI from June 2016. The patient died in July 2016. Adapted from the original publication of Lim et. al. (1)

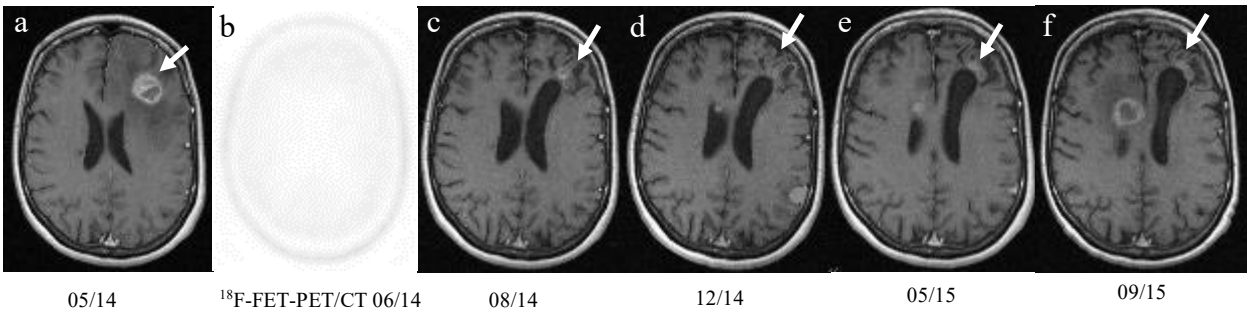

Figure 11. Patient with metastatic breast cancer

Serial contrast-enhanced MR images obtained after CK-RS with PET examination performed after detection of suspicious lesion in MRI: (a), (c) – (f) are contrast-enhanced T1-weighted MR images, (b) is a PET image.

Left frontal metastasis (arrow) was treated with CK-RS in June 2013. MRI follow-up in May 2014 (a) shows a suspicious lesion measuring 2.2 cm without uptake in the ^{18}F-FET-PET examination (b). Over the course of follow-up, the patient developed new brain metastases. The left frontal lesion is seen to show increasingly more pronounced enhancement starting in May 2015 (e). The patient died in January 2016. Adapted from the original publication of Lim et. al. (1)

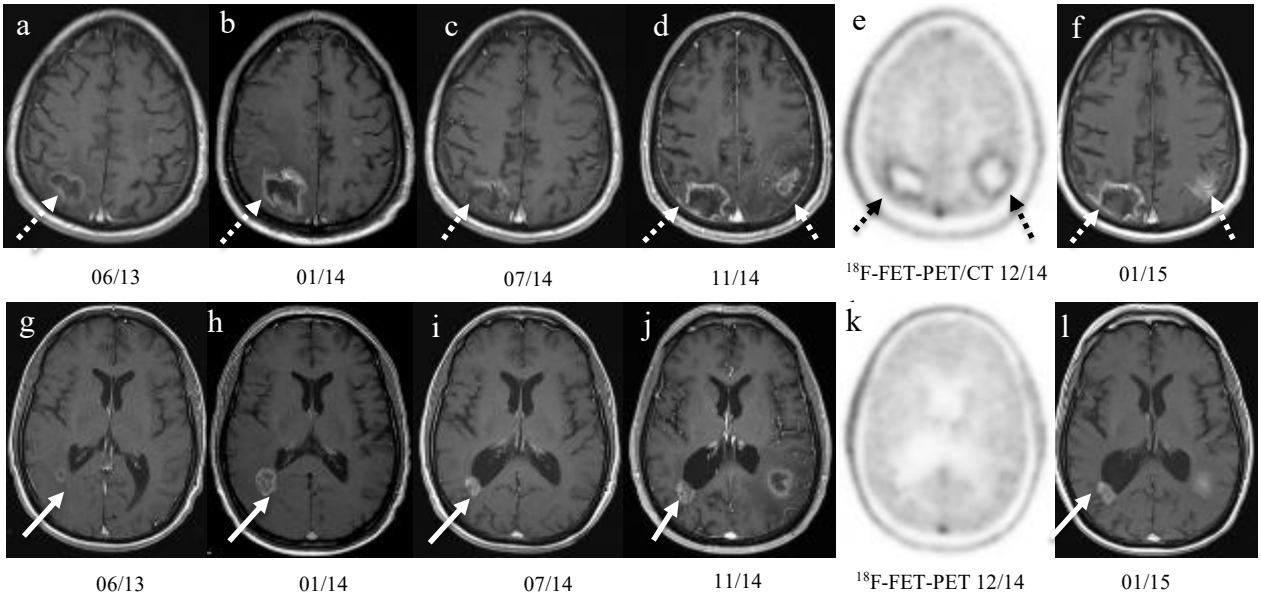

Figure 12. Patient with metastatic lung cancer

Serial contrast-enhanced MR images obtained after CK-RS with PET examination performed after detection of suspicious lesion in MRI: (e) and (k) depict PET acquisitions, the rest are post-contrast T1-weighted MRI images. Upper panel (a) – (f) shows two biparietal lesions (dotted arrows) over time. Lower panel (g) – (j) shows images from a more inferior plane taken at the same time points; the suspicious lesion in the lower panel is located posterior to the right posterior horn in (g) – (l) (white solid arrow).

The patient had whole brain radiotherapy in March 2012. The two biparietal lesions (dotted arrows) in the upper panel and the right posterior horn lesion in the lower panel (solid arrows) were treated with CK-RS in March 2013. These three lesions appeared suspicious from as early as June 2013. The biparietal lesions in (a) – (f) show circumferential tracer uptake in PET (e), while the right posterior horn lesion does not (k). The patient developed new left parietal metastasis in January 2014 which increased in size (not shown). There was only one cMRI done after the PET-examination (f) and (l), showing the right posterior horn lesion to be relatively stable. The patient died in hospice care in February 2015, approximately one month after the last cMRI. Adapted from the original publication of Lim et. al. (1)

4. Discussion

4.1. **Summary**

In this single-center study, the use of dynamic ^{18}F-FET-PET parameters led to a slight improvement of all diagnostic accuracy parameters analyzed, as already reported in Lim et al. (1). Overall, there was no combination of diagnostic parameters that provided both high sensitivity and high specificity. Specificity was particularly low, and the highest value reached in the study population was only 63%. Accuracy was highest when tracer uptake over time (TAC pattern) alone was used for differentiation of recurrent brain tumors from radionecrosis. Specificity alone was slightly improved when static and dynamic parameters were combined. Compared with the diagnostic probability of standard follow-up cMRI, post-test diagnostic probability of lesion differentiation using dynamic ^{18}F-FET PET/CT increased by 12% when all brain lesions in the study population were analyzed and by 16% in the subset of metastatic brain lesions (1). While this improvement in brain lesion differentiation is minor, our results clearly demonstrate the reproducibility and applicability of published cut-off values for dynamic ^{18}F-FET-PET parameters (88, 89, 98) in patients with primary and secondary brain lesions after CyberKnife treatment. All ^{18}F-FET-PET/CT diagnoses in the present study matched the histologic diagnoses available for 7 of the 28 lesions (25%) analyzed.

4.2. **Study Population Characteristics**

Our patient population was heterogenous, including both primary (n = 5) and secondary brain tumors (n = 23) (1). Conversely, most studies conducted so far investigated only either brain metastases or primary brain tumors (80, 85, 88-91, 93, 94, 98). For better comparability of the present findings with published data, separate analyses were conducted for all (primary and secondary) brain tumors (TOTAL) and the subset of metastatic lesions only (METS). All analyses carried out yielded similar results for the two groups, TOTAL and METS, which is predominantly attributable to the very small number of primary brain tumors (n = 5) in our study population.

The distribution of primary tumors underlying brain metastases in this study population (i.e., breast and lung cancer and melanoma) is consistent with the five most common primary cancers known to metastasize to the brain, i.e., lung and renal cancer, melanoma, breast and colorectal cancer (6, 7). Breast cancer was the most common primary tumor in our study population (9 of 14 patients, 60%) and had the shortest interval between CK-RS and dynamic ^{18}F-FET-PET/CT. This aligns with known clinical data: firstly, brain metastases are most frequent in breast and lung cancer patients (4, 9). Secondly, patients with brain metastases from breast cancer tend to have a poorer prognosis than patients with non-small-cell lung cancer as well as lower Karnofsky scores and more additional systemic metastases in other body regions (108).

The primary tumor entities (ependymoma and PTPR) in our study did not include glioblastoma – the most common primary brain tumor. This might be attributable to the exclusion criteria and the small size of the study population. Furthermore, patients with glioblastoma have short median survival estimates, ranging from around 7.5 to 17 months (109). SRS is a salvage treatment option for recurrent glioblastoma (110), and recurrence usually means a poorer prognosis. Posttherapeutic changes such as radionecrosis, however, may occur years after treatment. Thus, patients with glioblastoma might not have survived long enough to develop radionecrosis.

The fact that differences did not reach statistical significance in our study is likely also attributable to the small study population. The only significant difference in PET parameters between recurrent brain tumor and radionecrosis was found for TBR_{max} in the METS group ($p = 0.01$) and for TTP between lesions with TAC I (radionecrosis) versus TAC III (recurrent brain tumor) patterns. Nevertheless, the results of the diagnostic accuracy tests still lead to the hypothesis that dynamic ^{18}F-FET-PET/CT has comparative effectiveness in differentiating primary and secondary brain tumor recurrence from radionecrosis, supporting previously reported results for brain metastases and gliomas (85, 88-91, 93, 94). Further prospective studies investigating larger numbers of study population are needed to validate this hypothesis.

4.3. **CyberKnife® Treatment and Radionecrosis**

The most important factors contributing to the occurrence of radionecrosis include radiation dose, tumor volume, location of lesions within the brain, and fractionation. The incidence of radionecrosis can be as high as 50% in SRS treatment of brain metastases with a dose of 16 to 22 Gy. Single-dose radiotherapy has a radionecrosis rate of about 20% vs. 8% for fractionated therapy (70, 111-115). In general, SRS has a higher risk of radionecrosis than other types of radiotherapy (16, 66-68). SRS works by focusing radiation beams from different angles on a target point, causing microvascular defects that affect both malignant and normal cells and lead to reactive changes such as tissue inflammation and vessel impermeability (116). Perifocal edema, with or without contrast enhancement in cMRI, is a common reactive change in the brain. Such changes often look very similar to malignant processes, thus rendering cMRI unreliable in differentiating tumor progression from radionecrosis. Moreover, these post-SRS reactive changes are often asymptomatic. The latency period between imaging changes and possible clinical symptoms adds to the challenges clinicians face in differentiating tumor recurrence from radionecrosis. Reactive changes in cMRI typically appear 6 to 8 months after SRS, though a longer time period of 23 months has also been reported (116-118). In our study, the longest interval between the last CK-RS session and the PET examination was 35 months in TOTAL and 23 months in METS (1).

Minniti et al. (2011) recommend fractionation to avoid post-treatment changes after SRS when the total brain volume irradiated with 12 Gy is larger than 8.5 cm^3 (70). This recommendation is taken into account in routine clinical treatment planning in our department. In a study population most similar to ours, Zhuang et al. (2016) showed that the occurrence of radionecrosis after CyberKnife treatment of primary and secondary brain tumors was predominantly influenced by the biologically equivalent dose (BED), treatment fractionation, and previous WBRT. The authors found a BED threshold of 74 Gy to be the most effective predictor of radionecrosis and recommended a maximum dose of 22.68 Gy as dose per session in patients undergoing unfractionated radiation (119). Mean BED in our study was below this threshold with approx. 43 Gy for TOTAL and 64 Gy for METS. All treatments in our study were unfractionated, and irradiated volumes were relatively small, with a median PTV of 1.5 cm^3 in both TOTAL and METS

and a median GTV of 1.40 cm^3 in TOTAL and 1.50 cm^3 in METS. Mean PTV and GTV were 2.1 cm^3 in TOTAL and 2.4 cm^3 in METS. Mean and median prescription dose was 19 Gy (range of 13-20 Gy in TOTAL and 16-20 Gy in METS), which is in the range of standard doses reported by other authors (70, 111, 114, 115, 119).

Despite the limitations of our study, our findings provide valuable insights, especially in view of the fact that experience with the CyberKnife SRS system is still limited. Twelve centers have a CyberKnife system in Germany, and the system at the Charité was the first CyberKnife system installed in a teaching/university hospital in Germany (120-122).

4.4. **Assessment of ^{18}F-FET-PET Parameters**

As a molecular diagnostic imaging modality, PET detects conspicuous tracer uptake associated with pathological processes such as malignant tumors or inflammatory conditions. The amino acid tracer O-(2-[18F]fluoroethyl)-l-tyrosine (^{18}F-FET) is an artificial amino acid tagged with ^{18}F. With its high accumulation in brain tumors and low accumulation in inflammatory brain tissue, this tracer is widely used in PET examinations of brain tumor patients. Uptake of this tracer is also low in peripheral tumors, supposedly because of its specific transport mechanisms: ^{18}F-FET tracer uptake relies on the amino acid transporter system, in particular the L-transporter system, which consists of many subtypes and transports neutral amino acids (123). This transport system is active at the blood-brain barrier and is stereospecific, meaning that it only allows transport of L-isomers of ^{18}F-FET (87); see Section 1.3.

After intravenous injection, ^{18}F-FET typically accumulates in brain lesions, rendering them visible in PET. Because malignant lesions and benign processes have different tracer uptake patterns, the uptake pattern or curve theoretically allows lesion characterization such as differentiation of recurrent tumor from radiation necrosis. This assumption was confirmed by the trends observed in our study, though we did not obtain statistically significant results. In our study, dynamic parameters only slightly improved the diagnostic accuracy of ^{18}F-FET-PET/CT compared with static parameters. Accuracy was highest when only time-activity curves of tracer uptake over time were analyzed for differentiation (Figure 9). Combination with the additional dynamic parameter TTP did not improve post-

test diagnostic probability (Table 11). It is therefore of interest to further investigate whether the TAC pattern alone may be sufficient for brain lesion differentiation in the clinical setting.

However, identification of one of the three known TAC patterns is not always straightforward. In our study population, the typical TAC pattern III with a short and quick ascent followed by a steep descent and plateau described in previous publications (89, 92) was not unambiguously identifiable. Instead, flatter descending patterns, often followed by a plateau, were more common. This explains the atypical example of TAC pattern III presented in Figure 8.

There was no difference in median TTP between recurrent tumor and radionecrosis in the group of all brain lesions in our study population and the subset of metastatic brain lesions only, but mean TTP tended to be higher in radionecrosis, which is probably attributable to the high standard deviation. TTP ≥ 20 minutes was seen in 33% of radionecrosis lesions and 10% of recurrent tumors. In accordance with this distribution, ROC analysis of TTP yielded an atypical curve form with no reliable cut-off. Generally, there were mixed results for TTP distribution across TAC patterns, probably due to the small study population. Except for the pairwise comparison of TTP between TAC I and TAC III lesions in the group of all lesions, there was no significant TTP difference in other pairwise comparisons in TOTAL and no significant difference at all in METS. Nevertheless, TTP tended to be longer in TAC I lesions, or radionecrosis, than in malignant lesions with TAC II or III patterns. In their study from 2017, Unterrainer et al. concluded that, although cancerous lesions tend to have a TAC III tracer uptake pattern, there is high heterogeneity or variability in TAC patterns and TTP among metastases from different primary tumors, at least before treatment (124). This might explain why no reliable TTP cut-off values could be derived in our study or in the 2016 study of Romagna et al. (98). Along with the small study population, this might explain why our results possibly underestimate the true benefit of ^{18}F-FET-PET.

Another finding to be discussed is the occurrence of ^{18}F-FET-negative lesions in our study population (Section 3.2.4., Figures 10-12) (1). The negative glioblastoma presented in Figure 10 had decreasing contrast enhancement in serial MRI follow-up, thus confirming the diagnosis made by PET. This case nicely illustrates that PET can still help in lesion

differentiation even when a lesion shows no tracer uptake, which is due to the principle of molecular imaging and thus the in vivo characterization of lesions. However, interpretation of the other two cases (Figures 11 and 12) was challenging. Due to progressive disease, the patients' death, and the lack of further MR images, it is possible that either the suspicious lesions were initially tumor-free with recurrent tumor developing over time, or dynamic ^{18}F-FET-PET/CT failed to detect tumor at the time of examination. Several studies have shown that brain tumors can be ^{18}F-FET-negative, namely up to 30% of low-grade gliomas and up to 5% of high-grade gliomas as well as secondary brain tumors (125-128). Unterrainer et al. found high variation in uptake intensity among untreated brain metastases from different primary tumors and ^{18}F-FET negativity in small metastases (≤ 1.0 cm) from breast cancer and malignant melanoma (124). The three negative lesions in our study were larger than 1.0 cm in size and were a high-grade glioma and two metastatic lesions (from breast and lung cancer). In interpreting imaging findings, examiners must bear in mind that, after treatment of several brain lesions, a patient may have both, recurrent tumor and radionecrosis, in follow-up imaging.

4.5. **Performance of Diagnostic Parameters**

Although ^{18}F-FET-PET/CT correctly identified all seven histologically confirmed lesions in our study (Table 10), the best diagnostic accuracy achieved in this study was moderate with merely 75% sensitivity in both groups and specificity of 63% vs. 71%, LR+ 2.00 vs. 2.63, LR- 0.40 vs. 0.35, and post-test probability 83% vs. 86% in TOTAL vs. METS, respectively. These are the diagnostic accuracy values achieved with the combined use of TBR_{mean} and TAC pattern for lesion differentiation. In comparison, the highest published sensitivity and specificity in differentiating recurrent brain metastasis from radionecrosis were 95% and 93%, respectively – with a pooled sensitivity of 83% and pooled specificity of 89% (90, 91, 94, 96). As mentioned before, we performed the diagnostic accuracy tests using cut-off values derived from published data (Table 12). For TBR_{mean}, we chose the cut-off of 1.95, which was successfully reproduced by Galldiks et al. (2012), Romagna et al. (2016), and Ceccon et al. (2017) (88, 89, 97, 98) The non-significant cut-off for TBR_{mean} of 2.13 identified in our ROC curve analysis is relatively close to the value we used. For TTP, we used 20 minutes as threshold based on Galldiks

et al. (89), as it is closest to our own non-significant TTP cut-off of 25 minutes. Conversely, Ceccon et al. used a TTP threshold of 32.5 minutes, while Romagna et al. could not derive a reliable TTP threshold either (88, 98). As can be seen from Table 12, Guffens et al. (2015) was the only other study with a sensitivity < 80%. Li et al. (2018) attributed this low sensitivity to a smaller variation in primary tumors underlying brain metastases compared to other studies (97). This explanation also holds true for our study, which included only two primary tumor entities, and for the study of Guffens et al. (2015) with three primary cancer entities (129). Ceccon et al. (2017) also investigated brain metastases from only three different primary cancers; however, their study population was twice as large as ours (88). Compared to all other studies compiled in Table 12, our study investigated the smallest total number of both patients and lesions.

The highest published diagnostic accuracy was 100% sensitivity and specificity for glioma (88, 89, 97, 98). With only two patients with two different primary brain tumors and a total of 5 brain lesions in our study population, there was no point in doing a separate analysis for a primary brain tumor group (1).

Post-test diagnostic probabilities improved by approximately 12% and 16% in TOTAL and METS, respectively. Analysis of pre-/post-test probabilities was carried out using the "prevalence" of lesions suspicious for tumor recurrence in our study population, which does not represent the actual prevalence of recurrent tumor and/or radionecrosis after CK-RS treatment in a general patient population. However, it is important to emphasize that our study was carried out to explore the benefit of dynamic ^{18}F-FET-PET/CT in the differentiation of brain lesions after CK-RS and to estimate how much this index test could improve diagnostic probability in this particular patient population, building on the high diagnostic accuracies achieved with dynamic ^{18}F-FET-PET/CT parameters in previous studies (19, 88-91, 93, 94, 97, 130).

Table 12. Overview of studies investigating ^{18}F-FET PET/CT for differentiating radionecrosis and recurrent brain metastasis after radiotherapy

Study	Year	Age Range / Median (y)	Male/ Female	Primary Cancer	Treatment	Patients	Lesions	Study Design	Median Follow-Up (Months)	Standard Reference	Cut-Off Values	Diagnostic Accuracy (Se/Sp %)
Galldiks et al. (89)	2012	17-70/53 (mean)	5:26	Lung, breast, renal, colorectal, skin, bone	SRS, WBRT	31	40	P	12	H+CR	TAC II and III + **TBRmean > 1.95**	95/91
Guffens et al. (129)	2015	n.a.	n.a.	Breast, lung, head & neck	n.a.	29	39	R	n.a.	H+C	TAC II and III vs. TAC I	69/86
Romagna et al. (98)	2016	61.9	11:11	Lung, breast, renal, gastrointenstinal, skin	SRS, SBT	22	34	P	28.3	H+CR	Descending TACs + TBRmax > 2.15 + **TBRmean > 1.95**	93/84
Ceccon et al. (88)	2017	17-78/55 (mean)	14:48	Lung, breast, mixed cancer	SRS, WBRT, EFRT, brachytherapy	62	76	R	16	H+CR	**TBRmean > 1.95** + presence of TAC slope < 0.37 SUV/h	83/93
Lim et al.	2022	16-79/52	2:12	Breast, lung, skin, (ependymoma, PTPR)	SRS–CyberKnife, WBRT	12 (2)	23 (5)	R	9	H+CR	TAC II and III + TBRmean > 1.95 *	75/71

This table is modified from Li et al., 2018 (97) and partially adapted from Lim et. al. (1)

*Cut-off value taken from three published studies (bold in the table) due to non-significant TBRmean cut-off of 2.13.

Abbreviations
SRS: stereotactic radiosurgery, WBRT: whole brain radiotherapy, SBT: stereotactic iodine-125 brachytherapy, EFRT: external fractionated radiotherapy, P: prospective, R: retrospective, H+CR: histology+ clinicoradiological findings, H+C: histology + clinical TAC: time-activity curve, TBR: tumor-to-background ratio, SUV: standard uptake value, Se: sensitivity, Sp: specificity, n.a.: not applicable, PTPR: papillary tumor of pineal region.
Note
For comparability, the data for our study in the last row are for the METS group only (with results for primary brain tumors in gray in brackets).

4.6. **Limitations**

Major limitations of this study include its single-center and retrospective design, a small number of patients, and the lack of sample size calculation, making this study underpowered for statistical analysis. Thus, this is a hypothesis-generating study (1).

Since the installation of a PET/MRI system in our institution, PET/MRI has replaced PET/CT for differentiation of recurrent brain tumor and radionecrosis because of its superiority in terms of tissue contrast and brain lesion characterization. Therefore, it was not possible to recruit more patients for our study.

Although some patients had multiple lesions, we treated each lesion as an individual data point (1). This is the usual procedure in neuro-oncological studies, although such cases are essentially dependent cases and should not be treated as purely individual data points. This issue should be addressed with appropriate methodology in future studies. This limitation might have affected our significance results, because significance tests are supposed to be done in either dependent or independent data, and not in mixed data as in our study. Confidence intervals were therefore always presented in the analyses to derive estimates. While providing information on statistical significance, confidence intervals are less prone to misinterpretation related to sample size than p-values. In addition, confidence intervals are less dependent on statistical assumptions.

Despite the limitations just outlined, this small retrospective pilot study still provides essential information regarding the differentiation of tumor recurrence from radionecrosis using dynamic ^{18}F-FET-PET/CT after robotic radiosurgery. Interest in experience with CyberKnife radiosurgery is likely to increase with the wider use of this system. To our knowledge, this is the first dynamic ^{18}F-FET-PET/CT study investigating this specific patient population. We hope this study can help in the planning of future studies or meta-analyses to confirm or disprove the results presented here.

5. Conclusion and Outlook

In our analysis, dynamic ^{18}F-FET-PET/CT improved post-test diagnostic probability by 12%-16% in patients with suspected recurrent brain lesions after high-precision image-guided robotic stereotactic radiosurgery (CyberKnife®). This improvement was accomplished using a published cut-off value of TBR_{mean} > 1.95 and dynamic ^{18}F-FET-

PET parameters. Diagnostic accuracy was only moderate, with high sensitivity but low specificity. Accuracy was highest when time-activity curve (TAC) patterns were used as the only diagnostic parameter. Evaluation of TAC patterns alone as the best diagnostic parameter holds promise for improving accuracy and, if confirmed, might reduce the need for quantitative measurement of parameters such as TBR in the clinical setting. Larger prospective studies are warranted to validate our findings.

6. References

1. Lim W, Acker G, Hardt J, Kufeld M, Kluge A, Brenner W, Conti A, Budach V, Vajkoczy P, Senger C, Prasad V. Dynamic (18)F-FET PET/CT to differentiate recurrent primary brain tumor and brain metastases from radiation necrosis after single-session robotic radiosurgery. Cancer Treat Res Commun. 2022;32:100583.

2. Ostrom QT, Cioffi G, Waite K, Kruchko C, Barnholtz-Sloan JS. CBTRUS Statistical Report: Primary Brain and Other Central Nervous System Tumors Diagnosed in the United States in 2014-2018. Neuro Oncol. 2021;23(12 Suppl 2):iii1-iii105.

3. Gavrilovic IT, Posner JB. Brain metastases: epidemiology and pathophysiology. J Neurooncol. 2005;75(1):5-14.

4. Davis FG, Dolecek TA, McCarthy BJ, Villano JL. Toward determining the lifetime occurrence of metastatic brain tumors estimated from 2007 United States cancer incidence data. Neuro Oncol. 2012;14(9):1171-7.

5. Central Nervous System Cancers National Comprehensive Cancer Network®: NCCN Clinical Practice Guidelines in Oncology (NCCN Guidelines®) 2021 [updated September 08, 2021. Version 2.2021:[Available from: https://www.nccn.org/professionals/physician_gls/pdf/cns.pdf. Accessed March 1, 2022.

6. Barnholtz-Sloan JS, Sloan AE, Davis FG, Vigneau FD, Lai P, Sawaya RE. Incidence proportions of brain metastases in patients diagnosed (1973 to 2001) in the Metropolitan Detroit Cancer Surveillance System. J Clin Oncol. 2004;22(14):2865-72.

7. Schouten LJ, Rutten J, Huveneers HA, Twijnstra A. Incidence of brain metastases in a cohort of patients with carcinoma of the breast, colon, kidney, and lung and melanoma. Cancer. 2002;94(10):2698-705.

8. Cagney DN, Martin AM, Catalano PJ, Redig AJ, Lin NU, Lee EQ, Wen PY, Dunn IF, Bi WL, Weiss SE, Haas-Kogan DA, Alexander BM, Aizer AA. Incidence and prognosis of patients with brain metastases at diagnosis of systemic malignancy: a population-based study. Neuro Oncol. 2017;19(11):1511-21.

9. Budczies J, von Winterfeld M, Klauschen F, Bockmayr M, Lennerz JK, Denkert C, Wolf T, Warth A, Dietel M, Anagnostopoulos I, Weichert W, Wittschieber D, Stenzinger A. The landscape of metastatic progression patterns across major human cancers. Oncotarget. 2015;6(1):570-83.

10. Ostrom QT, Gittleman H, Liao P, Vecchione-Koval T, Wolinsky Y, Kruchko C, Barnholtz-Sloan JS. CBTRUS Statistical Report: Primary brain and other central nervous system tumors diagnosed in the United States in 2010-2014. Neuro Oncol. 2017;19(suppl_5):v1-v88.

11. Louis DN, Ohgaki H, Wiestler OD, Cavenee WK, Burger PC, Jouvet A, Scheithauer BW, Kleihues P. The 2007 WHO classification of tumours of the central nervous system. Acta Neuropathol. 2007;114(2):97-109.

12. Louis DN, Perry A, Reifenberger G, von Deimling A, Figarella-Branger D, Cavenee WK, Ohgaki H, Wiestler OD, Kleihues P, Ellison DW. The 2016 World Health Organization Classification of Tumors of the Central Nervous System: a summary. Acta Neuropathol. 2016;131(6):803-20.

13. Board WCoTE. World Health Organization Classification of Tumours of the Central Nervous System. Lyon; 2021.

14. Louis DN, Perry A, Wesseling P, Brat DJ, Cree IA, Figarella-Branger D, Hawkins C, Ng HK, Pfister SM, Reifenberger G, Soffietti R, von Deimling A, Ellison DW. The 2021 WHO Classification of Tumors of the Central Nervous System: a summary. Neuro Oncol. 2021;23(8):1231-51.

15. Lapointe S, Perry A, Butowski NA. Primary brain tumours in adults. Lancet. 2018;392(10145):432-46.

16. Soffietti R, Abacioglu U, Baumert B, Combs SE, Kinhult S, Kros JM, Marosi C, Metellus P, Radbruch A, Villa Freixa SS, Brada M, Carapella CM, Preusser M, Le Rhun E, Rudà R, Tonn JC, Weber DC, Weller M. Diagnosis and treatment of brain metastases from solid tumors: guidelines from the European Association of Neuro-Oncology (EANO). Neuro-Oncology. 2017;19(2):162-74.

17. Galicich JH, French LA, Melby JC. Use of dexamethasone in treatment of cerebral edema associated with brain tumors. J Lancet. 1961;81:46-53.

18. Schiff D, Lee EQ, Nayak L, Norden AD, Reardon DA, Wen PY. Medical management of brain tumors and the sequelae of treatment. Neuro Oncol. 2015;17(4):488-504.

19. Galldiks N, Law I, Pope WB, Arbizu J, Langen KJ. The use of amino acid PET and conventional MRI for monitoring of brain tumor therapy. Neuroimage Clin. 2017;13:386-94.

20. Chaichana KL, Jusue-Torres I, Navarro-Ramirez R, Raza SM, Pascual-Gallego M, Ibrahim A, Hernandez-Hermann M, Gomez L, Ye X, Weingart JD, Olivi A, Blakeley J, Gallia GL, Lim M, Brem H, Quinones-Hinojosa A. Establishing percent resection and residual volume thresholds affecting survival and recurrence for patients with newly diagnosed intracranial glioblastoma. Neuro Oncol. 2014;16(1):113-22.

21. Lacroix M, Abi-Said D, Fourney DR, Gokaslan ZL, Shi W, DeMonte F, Lang FF, McCutcheon IE, Hassenbusch SJ, Holland E, Hess K, Michael C, Miller D, Sawaya R. A multivariate analysis of 416 patients with glioblastoma multiforme: prognosis, extent of resection, and survival. J Neurosurg. 2001;95(2):190-8.

22. Timur Mitin M, PhD. Radiation therapy techniques in cancer treatment. In: Sadhna R Vora M, editor. UpToDate, Waltham, MA. (Accessed on February 23, 2019): *UpToDate*; 2017.

23. Filley AC, Dey M. Dendritic cell based vaccination strategy: an evolving paradigm. J Neurooncol. 2017;133(2):223-35.

24. Weller M, Roth P, Preusser M, Wick W, Reardon DA, Platten M, Sampson JH. Vaccine-based immunotherapeutic approaches to gliomas and beyond. Nat Rev Neurol. 2017;13(6):363-74.

25. Lang FF, Conrad C, Gomez-Manzano C, Yung WKA, Sawaya R, Weinberg JS, Prabhu SS, Rao G, Fuller GN, Aldape KD, Gumin J, Vence LM, Wistuba I, Rodriguez-Canales J, Villalobos PA, Dirven CMF, Tejada S, Valle RD, Alonso MM, Ewald B, Peterkin JJ, Tufaro F, Fueyo J. Phase I Study of DNX-2401 (Delta-24-RGD) Oncolytic Adenovirus: Replication and Immunotherapeutic Effects in Recurrent Malignant Glioma. J Clin Oncol. 2018;36(14):1419-27.

26. Gardeck AM, Sheehan J, Low WC. Immune and viral therapies for malignant primary brain tumors. Expert Opin Biol Ther. 2017;17(4):457-74.

27. Huang J, Liu F, Liu Z, Tang H, Wu H, Gong Q, Chen J. Immune Checkpoint in Glioblastoma: Promising and Challenging. Front Pharmacol. 2017;8:242.

28. Bagley SJ, Desai AS, Linette GP, June CH, O'Rourke DM. CAR T-cell therapy for glioblastoma: recent clinical advances and future challenges. Neuro Oncol. 2018;20(11):1429-38.

29. Zhao HF, Wang J, Shao W, Wu CP, Chen ZP, To ST, Li WP. Recent advances in the use of PI3K inhibitors for glioblastoma multiforme: current preclinical and clinical development. Mol Cancer. 2017;16(1):100.

30. Goetz P, Ebinu JO, Roberge D, Zadeh G. Current standards in the management of cerebral metastases. Int J Surg Oncol. 2012;2012:493426.

31. Kamar FG, Posner JB. Brain metastases. Semin Neurol. 2010;30(3):217-35.

32. Sperduto PW, Chao ST, Sneed PK, Luo X, Suh J, Roberge D, Bhatt A, Jensen AW, Brown PD, Shih H, Kirkpatrick J, Schwer A, Gaspar LE, Fiveash JB, Chiang V, Knisely J, Sperduto CM, Mehta M. Diagnosis-specific prognostic factors, indexes, and treatment outcomes for patients with newly diagnosed brain metastases: a multi-institutional analysis of 4,259 patients. Int J Radiat Oncol Biol Phys. 2010;77(3):655-61.

33. Sperduto PW. What is your patient's GPA and why does it matter? Managing brain metastases and the cost of hope. Int J Radiat Oncol Biol Phys. 2010;77(3):643-4.

34. Sperduto PW, Kased N, Roberge D, Xu Z, Shanley R, Luo X, Sneed PK, Chao ST, Weil RJ, Suh J, Bhatt A, Jensen AW, Brown PD, Shih HA, Kirkpatrick J, Gaspar LE,

Fiveash JB, Chiang V, Knisely JP, Sperduto CM, Lin N, Mehta M. Summary report on the graded prognostic assessment: an accurate and facile diagnosis-specific tool to estimate survival for patients with brain metastases. J Clin Oncol. 2012;30(4):419-25.

35. Gaspar L, Scott C, Rotman M, Asbell S, Phillips T, Wasserman T, McKenna WG, Byhardt R. Recursive partitioning analysis (RPA) of prognostic factors in three Radiation Therapy Oncology Group (RTOG) brain metastases trials. Int J Radiat Oncol Biol Phys. 1997;37(4):745-51.

36. Patchell RA, Tibbs PA, Regine WF, Dempsey RJ, Mohiuddin M, Kryscio RJ, Markesbery WR, Foon KA, Young B. Postoperative radiotherapy in the treatment of single metastases to the brain: a randomized trial. JAMA. 1998;280(17):1485-9.

37. Soon YY, Tham IW, Lim KH, Koh WY, Lu JJ. Surgery or radiosurgery plus whole brain radiotherapy versus surgery or radiosurgery alone for brain metastases. Cochrane Database Syst Rev. 2014(3):CD009454.

38. Brown PD, Jaeckle K, Ballman KV, Farace E, Cerhan JH, Anderson SK, Carrero XW, Barker FG, 2nd, Deming R, Burri SH, Menard C, Chung C, Stieber VW, Pollock BE, Galanis E, Buckner JC, Asher AL. Effect of Radiosurgery Alone vs Radiosurgery With Whole Brain Radiation Therapy on Cognitive Function in Patients With 1 to 3 Brain Metastases: A Randomized Clinical Trial. JAMA. 2016;316(4):401-9.

39. Chang EL, Wefel JS, Hess KR, Allen PK, Lang FF, Kornguth DG, Arbuckle RB, Swint JM, Shiu AS, Maor MH, Meyers CA. Neurocognition in patients with brain metastases treated with radiosurgery or radiosurgery plus whole-brain irradiation: a randomised controlled trial. Lancet Oncol. 2009;10(11):1037-44.

40. Medical Subject Headings (MeSH) Database. Radiotherapy [Available from: https://www.ncbi.nlm.nih.gov/mesh/68011878. Accessed February 22, 2021.

41. Withers HR. The Four R's of Radiotherapy. In: Lett JT, Adler H, editors. Adv Radiat Biol. 5: Elsevier; 1975. p. 241-71.

42. Elkind MM, Sutton-Gilbert H, Moses WB, Alescio T, Swain RW. Radiation Response of Mammalian Cells Grown in Culture. V. Temperature Dependence of the Repair of X-Ray Damage in Surviving Cells (Aerobic and Hypoxic). Radiat Res. 1965;25:359-76.

43. Bernier J, Hall EJ, Giaccia A. Radiation oncology: a century of achievements. Nat Rev Cancer. 2004;4(9):737-47.

44. Chan A CR, Loeffler J. . Stereotactic irradiation. In: Perez CA BL, Halperin CA, Schmidt-Ullrich RK, editor. Principles and practice of radiation oncology Lippincott Williams & Wilkins, Philadelphia 2004.

45. Clark C Chen M, PhD; Paul H Chapman, MD; Jay S Loeffler, MD. Steretotactic cranial radiosurgery. In: Sadhna R Vora M, editor. UpToDate, Waltham, MA. (Accessed on November 26, 2020): *UpToDate*; 2019.

46. Leksell L. The stereotaxic method and radiosurgery of the brain. Acta Chir Scand. 1951;102(4):316-9.

47. Leksell L. Stereotactic radiosurgery. J Neurol Neurosurg Psychiatry. 1983;46(9):797-803.

48. Medical Subject Headings (MeSH) Database. Radiosurgery [Available from: https://www.ncbi.nlm.nih.gov/mesh/?term=radiosurgery. Accessed February 22, 2021.

49. Kaul D, Badakhshi H, Gevaert T, Pasemann D, Budach V, Tuleasca C, Gruen A, Prasad V, Levivier M, Kufeld M. Dosimetric comparison of different treatment modalities for stereotactic radiosurgery of meningioma. Acta Neurochir (Wien). 2015;157(4):559-63; discussion 63-4.

50. Stereotactic Radiosurgery and Stereotactic Body Radiation Therapy: Springer International Publishing; 2019.

51. Adler JR, Jr., Chang SD, Murphy MJ, Doty J, Geis P, Hancock SL. The Cyberknife: a frameless robotic system for radiosurgery. Stereotact Funct Neurosurg. 1997;69(1-4 Pt 2):124-8.

52. Kuo JS, Yu C, Petrovich Z, Apuzzo ML. The CyberKnife stereotactic radiosurgery system: description, installation, and an initial evaluation of use and functionality. Neurosurgery. 2003;53(5):1235-9; discussion 9.

53. Chang SD, Adler JR. Robotics and radiosurgery - The cyberknife. Stereotact Funct Neurosurg. 2001;76(3-4):204-8.

54. Adler JR, Jr., Murphy MJ, Chang SD, Hancock SL. Image-guided robotic radiosurgery. Neurosurgery. 1999;44(6):1299-306; discussion 306-7.

55. Acker G, Meinert F, Conti A, Kufeld M, Jelgersma C, Nguyen P, Kluge A, Lukas M, Loebel F, Pasemann D, Kaul D, Budach V, Vajkoczy P, Senger C. Image-Guided Robotic Radiosurgery for Treatment of Recurrent Grade II and III Meningiomas. A Single-Center Study. World Neurosurg. 2019;131:e96-e107.

56. Wen PY, Macdonald DR, Reardon DA, Cloughesy TF, Sorensen AG, Galanis E, Degroot J, Wick W, Gilbert MR, Lassman AB, Tsien C, Mikkelsen T, Wong ET, Chamberlain MC, Stupp R, Lamborn KR, Vogelbaum MA, van den Bent MJ, Chang SM. Updated response assessment criteria for high-grade gliomas: response assessment in neuro-oncology working group. J Clin Oncol. 2010;28(11):1963-72.

57. van den Bent MJ, Wefel JS, Schiff D, Taphoorn MJ, Jaeckle K, Junck L, Armstrong T, Choucair A, Waldman AD, Gorlia T, Chamberlain M, Baumert BG, Vogelbaum

MA, Macdonald DR, Reardon DA, Wen PY, Chang SM, Jacobs AH. Response assessment in neuro-oncology (a report of the RANO group): assessment of outcome in trials of diffuse low-grade gliomas. Lancet Oncol. 2011;12(6):583-93.

58. Lin NU, Lee EQ, Aoyama H, Barani IJ, Barboriak DP, Baumert BG, Bendszus M, Brown PD, Camidge DR, Chang SM, Dancey J, de Vries EG, Gaspar LE, Harris GJ, Hodi FS, Kalkanis SN, Linskey ME, Macdonald DR, Margolin K, Mehta MP, Schiff D, Soffietti R, Suh JH, van den Bent MJ, Vogelbaum MA, Wen PY, Response Assessment in Neuro-Oncology g. Response assessment criteria for brain metastases: proposal from the RANO group. Lancet Oncol. 2015;16(6):e270-8.

59. Huang C, McConathy J. Radiolabeled amino acids for oncologic imaging. J Nucl Med. 2013;54(7):1007-10.

60. Sheline GE, Wara WM, Smith V. Therapeutic irradiation and brain injury. Int J Radiat Oncol Biol Phys. 1980;6(9):1215-28.

61. Werner-Wasik M, Rudoler S, Preston PE, Hauck WW, Downes BM, Leeper D, Andrews D, Corn BW, Curran WJ, Jr. Immediate side effects of stereotactic radiotherapy and radiosurgery. Int J Radiat Oncol Biol Phys. 1999;43(2):299-304.

62. Brandsma D, Stalpers L, Taal W, Sminia P, van den Bent MJ. Clinical features, mechanisms, and management of pseudoprogression in malignant gliomas. Lancet Oncol. 2008;9(5):453-61.

63. Powell C, Guerrero D, Sardell S, Cumins S, Wharram B, Traish D, Gonsalves A, Ashley S, Brada M. Somnolence syndrome in patients receiving radical radiotherapy for primary brain tumours: a prospective study. Radiother Oncol. 2011;100(1):131-6.

64. Lawenda BD, Gagne HM, Gierga DP, Niemierko A, Wong WM, Tarbell NJ, Chen GT, Hochberg FH, Loeffler JS. Permanent alopecia after cranial irradiation: dose-response relationship. Int J Radiat Oncol Biol Phys. 2004;60(3):879-87.

65. Shah AH, Snelling B, Bregy A, Patel PR, Tememe D, Bhatia R, Sklar E, Komotar RJ. Discriminating radiation necrosis from tumor progression in gliomas: a systematic review what is the best imaging modality? J Neurooncol. 2013;112(2):141-52.

66. Donovan EK, Parpia S, Greenspoon JN. Incidence of radionecrosis in single-fraction radiosurgery compared with fractionated radiotherapy in the treatment of brain metastasis. Curr Oncol. 2019;26(3):e328-e33.

67. Ling DC, Vargo JA, Wegner RE, Flickinger JC, Burton SA, Engh J, Amankulor N, Quinn AE, Ozhasoglu C, Heron DE. Postoperative stereotactic radiosurgery to the resection cavity for large brain metastases: clinical outcomes, predictors of intracranial failure, and implications for optimal patient selection. Neurosurgery. 2015;76(2):150-6; discussion 6-7; quiz 7.

68. Minniti G, Esposito V, Clarke E, Scaringi C, Lanzetta G, Salvati M, Raco A, Bozzao A, Maurizi Enrici R. Multidose stereotactic radiosurgery (9 Gy x 3) of the postoperative resection cavity for treatment of large brain metastases. Int J Radiat Oncol Biol Phys. 2013;86(4):623-9.

69. Sneed PK, Mendez J, Vemer-van den Hoek JG, Seymour ZA, Ma L, Molinaro AM, Fogh SE, Nakamura JL, McDermott MW. Adverse radiation effect after stereotactic radiosurgery for brain metastases: incidence, time course, and risk factors. J Neurosurg. 2015;123(2):373-86.

70. Minniti G, Clarke E, Lanzetta G, Osti MF, Trasimeni G, Bozzao A, Romano A, Enrici RM. Stereotactic radiosurgery for brain metastases: analysis of outcome and risk of brain radionecrosis. Radiat Oncol. 2011;6:48.

71. Verger A, Kas A, Darcourt J, Guedj E. PET Imaging in Neuro-Oncology: An Update and Overview of a Rapidly Growing Area. Cancers (Basel). 2022;14(5).

72. Shields AF, Grierson JR, Dohmen BM, Machulla HJ, Stayanoff JC, Lawhorn-Crews JM, Obradovich JE, Muzik O, Mangner TJ. Imaging proliferation in vivo with [F-18]FLT and positron emission tomography. Nat Med. 1998;4(11):1334-6.

73. Delbeke D. Oncological applications of FDG PET imaging: brain tumors, colorectal cancer, lymphoma and melanoma. J Nucl Med. 1999;40(4):591-603.

74. Becherer A, Karanikas G, Szabo M, Zettinig G, Asenbaum S, Marosi C, Henk C, Wunderbaldinger P, Czech T, Wadsak W, Kletter K. Brain tumour imaging with PET: a comparison between [18F]fluorodopa and [11C]methionine. Eur J Nucl Med Mol Imaging. 2003;30(11):1561-7.

75. Antinori A, De Rossi G, Ammassari A, Cingolani A, Murri R, Di Giuda D, De Luca A, Pierconti F, Tartaglione T, Scerrati M, Larocca LM, Ortona L. Value of combined approach with thallium-201 single-photon emission computed tomography and Epstein-Barr virus DNA polymerase chain reaction in CSF for the diagnosis of AIDS-related primary CNS lymphoma. J Clin Oncol. 1999;17(2):554-60.

76. Di Chiro G, DeLaPaz RL, Brooks RA, Sokoloff L, Kornblith PL, Smith BH, Patronas NJ, Kufta CV, Kessler RM, Johnston GS, Manning RG, Wolf AP. Glucose utilization of cerebral gliomas measured by [18F] fluorodeoxyglucose and positron emission tomography. Neurology. 1982;32(12):1323-9.

77. Di Chiro G, Brooks RA, Patronas NJ, Bairamian D, Kornblith PL, Smith BH, Mansi L, Barker J. Issues in the in vivo measurement of glucose metabolism of human central nervous system tumors. Ann Neurol. 1984;15 Suppl:S138-46.

78. McConathy J, Yu W, Jarkas N, Seo W, Schuster DM, Goodman MM. Radiohalogenated nonnatural amino acids as PET and SPECT tumor imaging agents. Med Res Rev. 2012;32(4):868-905.

79. Singhal T, Narayanan TK, Jain V, Mukherjee J, Mantil J. 11C-L-methionine positron emission tomography in the clinical management of cerebral gliomas. Mol Imaging Biol. 2008;10(1):1-18.

80. Dunet V, Rossier C, Buck A, Stupp R, Prior JO. Performance of 18F-fluoro-ethyl-tyrosine (18F-FET) PET for the differential diagnosis of primary brain tumor: a systematic review and Metaanalysis. J Nucl Med. 2012;53(2):207-14.

81. Bustany P, Chatel M, Derlon JM, Darcel F, Sgouropoulos P, Soussaline F, Syrota A. Brain tumor protein synthesis and histological grades: a study by positron emission tomography (PET) with C11-L-Methionine. J Neurooncol. 1986;3(4):397-404.

82. Ericson K, Lilja A, Bergstrom M, Collins VP, Eriksson L, Ehrin E, von Holst H, Lundqvist H, Langsrom BB, Mosskin M. Positron emission tomography with ([11C]methyl)-L-methionine, [11C]D-glucose, and [68Ga]EDTA in supratentorial tumors. J Comput Assist Tomogr. 1985;9(4):683-9.

83. Stegmayr C, Bandelow U, Oliveira D, Lohmann P, Willuweit A, Filss C, Galldiks N, Lubke JH, Shah NJ, Ermert J, Langen KJ. Influence of blood-brain barrier permeability on O-(2-(18)F-fluoroethyl)-L-tyrosine uptake in rat gliomas. Eur J Nucl Med Mol Imaging. 2017;44(3):408-16.

84. Gotz I, Grosu AL. [(18)F]FET-PET Imaging for Treatment and Response Monitoring of Radiation Therapy in Malignant Glioma Patients - A Review. Front Oncol. 2013;3:104.

85. Bashir A, Mathilde Jacobsen S, Molby Henriksen O, Broholm H, Urup T, Grunnet K, Andree Larsen V, Moller S, Skjoth-Rasmussen J, Skovgaard Poulsen H, Law I. Recurrent glioblastoma versus late posttreatment changes: diagnostic accuracy of O-(2-[18F]fluoroethyl)-L-tyrosine positron emission tomography (18F-FET PET). Neuro Oncol. 2019.

86. Langen KJ, Jarosch M, Muhlensiepen H, Hamacher K, Broer S, Jansen P, Zilles K, Coenen HH. Comparison of fluorotyrosines and methionine uptake in F98 rat gliomas. Nucl Med Biol. 2003;30(5):501-8.

87. Wester HJ, Herz M, Weber W, Heiss P, Senekowitsch-Schmidtke R, Schwaiger M, Stocklin G. Synthesis and radiopharmacology of O-(2-[18F]fluoroethyl)-L-tyrosine for tumor imaging. J Nucl Med. 1999;40(1):205-12.

88. Ceccon G, Lohmann P, Stoffels G, Judov N, Filss CP, Rapp M, Bauer E, Hamisch C, Ruge MI, Kocher M, Kuchelmeister K, Sellhaus B, Sabel M, Fink GR, Shah NJ, Langen KJ, Galldiks N. Dynamic O-(2-18F-fluoroethyl)-L-tyrosine positron emission tomography differentiates brain metastasis recurrence from radiation injury after radiotherapy. Neuro Oncol. 2017;19(2):281-8.

89. Galldiks N, Stoffels G, Filss CP, Piroth MD, Sabel M, Ruge MI, Herzog H, Shah NJ, Fink GR, Coenen HH, Langen KJ. Role of O-(2-(18)F-fluoroethyl)-L-tyrosine PET

for differentiation of local recurrent brain metastasis from radiation necrosis. J Nucl Med. 2012;53(9):1367-74.

90. Galldiks N, Stoffels G, Filss C, Rapp M, Blau T, Tscherpel C, Ceccon G, Dunkl V, Weinzierl M, Stoffel M, Sabel M, Fink GR, Shah NJ, Langen KJ. The use of dynamic O-(2-18F-fluoroethyl)-l-tyrosine PET in the diagnosis of patients with progressive and recurrent glioma. Neuro Oncol. 2015;17(9):1293-300.

91. Galldiks N, Stoffels G, Ruge MI, Rapp M, Sabel M, Reifenberger G, Erdem Z, Shah NJ, Fink GR, Coenen HH, Langen KJ. Role of O-(2-18F-fluoroethyl)-L-tyrosine PET as a diagnostic tool for detection of malignant progression in patients with low-grade glioma. J Nucl Med. 2013;54(12):2046-54.

92. Calcagni ML, Galli G, Giordano A, Taralli S, Anile C, Niesen A, Baum RP. Dynamic O-(2-[18F]fluoroethyl)-L-tyrosine (F-18 FET) PET for glioma grading: assessment of individual probability of malignancy. Clin Nucl Med. 2011;36(10):841-7.

93. Galldiks N, Dunkl V, Stoffels G, Hutterer M, Rapp M, Sabel M, Reifenberger G, Kebir S, Dorn F, Blau T, Herrlinger U, Hau P, Ruge MI, Kocher M, Goldbrunner R, Fink GR, Drzezga A, Schmidt M, Langen KJ. Diagnosis of pseudoprogression in patients with glioblastoma using O-(2-[18F]fluoroethyl)-L-tyrosine PET. Eur J Nucl Med Mol Imaging. 2015;42(5):685-95.

94. Kebir S, Fimmers R, Galldiks N, Schafer N, Mack F, Schaub C, Stuplich M, Niessen M, Tzaridis T, Simon M, Stoffels G, Langen KJ, Scheffler B, Glas M, Herrlinger U. Late Pseudoprogression in Glioblastoma: Diagnostic Value of Dynamic O-(2-[18F]fluoroethyl)-L-Tyrosine PET. Clin Cancer Res. 2016;22(9):2190-6.

95. Mihovilovic MI, Kertels O, Hanscheid H, Lohr M, Monoranu CM, Kleinlein I, Samnick S, Kessler AF, Linsenmann T, Ernestus RI, Buck AK, Lapa C. O-(2-((18)F)fluoroethyl)-L-tyrosine PET for the differentiation of tumour recurrence from late pseudoprogression in glioblastoma. J Neurol Neurosurg Psychiatry. 2019;90(2):238-9.

96. Rachinger W, Goetz C, Popperl G, Gildehaus FJ, Kreth FW, Holtmannspotter M, Herms J, Koch W, Tatsch K, Tonn JC. Positron emission tomography with O-(2-[18F]fluoroethyl)-l-tyrosine versus magnetic resonance imaging in the diagnosis of recurrent gliomas. Neurosurgery. 2005;57(3):505-11; discussion -11.

97. Li H, Deng L, Bai HX, Sun J, Cao Y, Tao Y, States LJ, Farwell MD, Zhang P, Xiao B, Yang L. Diagnostic Accuracy of Amino Acid and FDG-PET in Differentiating Brain Metastasis Recurrence from Radionecrosis after Radiotherapy: A Systematic Review and Meta-Analysis. AJNR Am J Neuroradiol. 2018;39(2):280-8.

98. Romagna A, Unterrainer M, Schmid-Tannwald C, Brendel M, Tonn JC, Nachbichler SB, Muacevic A, Bartenstein P, Kreth FW, Albert NL. Suspected recurrence of brain metastases after focused high dose radiotherapy: can [18F]FET- PET overcome diagnostic uncertainties? Radiat Oncol. 2016;11(1):139.

99. Bossuyt PM, Reitsma JB, Bruns DE, Gatsonis CA, Glasziou PP, Irwig L, Lijmer JG, Moher D, Rennie D, de Vet HC, Kressel HY, Rifai N, Golub RM, Altman DG, Hooft L, Korevaar DA, Cohen JF, Group S. STARD 2015: An Updated List of Essential Items for Reporting Diagnostic Accuracy Studies. Radiology. 2015;277(3):826-32.

100. Lohkamp LN, Vajkoczy P, Budach V, Kufeld M. Efficacy, safety and outcome of frameless image-guided robotic radiosurgery for brain metastases after whole brain radiotherapy. J Neurooncol. 2018;138(1):73-81.

101. Chang SD, Main W, Martin DP, Gibbs IC, Heilbrun MP. An analysis of the accuracy of the CyberKnife: a robotic frameless stereotactic radiosurgical system. Neurosurgery. 2003;52(1):140-6; discussion 6-7.

102. Charité Cyberknife Center.

103. Janssen JC, Woythal N, Meissner S, Prasad V, Brenner W, Diederichs G, Hamm B, Makowski MR. [(68)Ga]PSMA-HBED-CC Uptake in Osteolytic, Osteoblastic, and Bone Marrow Metastases of Prostate Cancer Patients. Mol Imaging Biol. 2017;19(6):933-43.

104. Macdonald DR, Cascino TL, Schold SC, Jr., Cairncross JG. Response criteria for phase II studies of supratentorial malignant glioma. J Clin Oncol. 1990;8(7):1277-80.

105. du Prel JB, Hommel G, Rohrig B, Blettner M. Confidence interval or p-value?: part 4 of a series on evaluation of scientific publications. Dtsch Arztebl Int. 2009;106(19):335-9.

106. Greenland S, Senn SJ, Rothman KJ, Carlin JB, Poole C, Goodman SN, Altman DG. Statistical tests, P values, confidence intervals, and power: a guide to misinterpretations. Eur J Epidemiol. 2016;31(4):337-50.

107. Cohen J. A power primer. Psychol Bull. 1992;112(1):155-9.

108. Aoyama H. Radiation therapy for brain metastases in breast cancer patients. Breast Cancer. 2011;18(4):244-51.

109. Li J, Wang M, Won M, Shaw EG, Coughlin C, Curran WJ, Jr., Mehta MP. Validation and simplification of the Radiation Therapy Oncology Group recursive partitioning analysis classification for glioblastoma. Int J Radiat Oncol Biol Phys. 2011;81(3):623-30.

110. Combs SE, Widmer V, Thilmann C, Hof H, Debus J, Schulz-Ertner D. Stereotactic radiosurgery (SRS): treatment option for recurrent glioblastoma multiforme (GBM). Cancer. 2005;104(10):2168-73.

111. Blonigen BJ, Steinmetz RD, Levin L, Lamba MA, Warnick RE, Breneman JC. Irradiated volume as a predictor of brain radionecrosis after linear accelerator stereotactic radiosurgery. Int J Radiat Oncol Biol Phys. 2010;77(4):996-1001.

112. Korytko T, Radivoyevitch T, Colussi V, Wessels BW, Pillai K, Maciunas RJ, Einstein DB. 12 Gy gamma knife radiosurgical volume is a predictor for radiation necrosis in non-AVM intracranial tumors. Int J Radiat Oncol Biol Phys. 2006;64(2):419-24.

113. Petrovich Z, Yu C, Giannotta SL, O'Day S, Apuzzo ML. Survival and pattern of failure in brain metastasis treated with stereotactic gamma knife radiosurgery. J Neurosurg. 2002;97(5 Suppl):499-506.

114. Shaw E, Scott C, Souhami L, Dinapoli R, Kline R, Loeffler J, Farnan N. Single dose radiosurgical treatment of recurrent previously irradiated primary brain tumors and brain metastases: final report of RTOG protocol 90-05. Int J Radiat Oncol Biol Phys. 2000;47(2):291-8.

115. Voges J, Treuer H, Sturm V, Buchner C, Lehrke R, Kocher M, Staar S, Kuchta J, Muller RP. Risk analysis of linear accelerator radiosurgery. Int J Radiat Oncol Biol Phys. 1996;36(5):1055-63.

116. Walker AJ, Ruzevick J, Malayeri AA, Rigamonti D, Lim M, Redmond KJ, Kleinberg L. Postradiation imaging changes in the CNS: how can we differentiate between treatment effect and disease progression? Future Oncol. 2014;10(7):1277-97.

117. Patel TR, McHugh BJ, Bi WL, Minja FJ, Knisely JP, Chiang VL. A comprehensive review of MR imaging changes following radiosurgery to 500 brain metastases. AJNR Am J Neuroradiol. 2011;32(10):1885-92.

118. Stockham AL, Tievsky AL, Koyfman SA, Reddy CA, Suh JH, Vogelbaum MA, Barnett GH, Chao ST. Conventional MRI does not reliably distinguish radiation necrosis from tumor recurrence after stereotactic radiosurgery. J Neurooncol. 2012;109(1):149-58.

119. Zhuang H, Zheng Y, Wang J, Chang JY, Wang X, Yuan Z, Wang P. Analysis of risk and predictors of brain radiation necrosis after radiosurgery. Oncotarget. 2016;7(7):7773-9.

120. Wikipedia. Cyberknife. Wikipedia, The Free Encyclopedia [updated December 5, 2020, 07:04 UTC. Available from: https://de.wikipedia.org/w/index.php?title=Cyberknife&oldid=206242238. Accessed February 21, 2021.

121. Department of Radiation Oncology and Radiotherapy: Charité – Universitätsmedizin Berlin. ; 2020 [Available from: https://radioonkologie.charite.de/en/services/cyberknife/. Accessed February 21, 2021.

122. CyberKnife Treatment Centers [Available from: https://cyberknife.com/treatment-centers/.

123. Langen KJ, Hamacher K, Weckesser M, Floeth F, Stoffels G, Bauer D, Coenen HH, Pauleit D. O-(2-[18F]fluoroethyl)-L-tyrosine: uptake mechanisms and clinical applications. Nucl Med Biol. 2006;33(3):287-94.

124. Unterrainer M, Galldiks N, Suchorska B, Kowalew LC, Wenter V, Schmid-Tannwald C, Niyazi M, Bartenstein P, Langen KJ, Albert NL. (18)F-FET PET Uptake Characteristics in Patients with Newly Diagnosed and Untreated Brain Metastasis. J Nucl Med. 2017;58(4):584-9.

125. Jansen NL, Graute V, Armbruster L, Suchorska B, Lutz J, Eigenbrod S, Cumming P, Bartenstein P, Tonn JC, Kreth FW, la Fougere C. MRI-suspected low-grade glioma: is there a need to perform dynamic FET PET? Eur J Nucl Med Mol Imaging. 2012;39(6):1021-9.

126. Jansen NL, Suchorska B, Wenter V, Eigenbrod S, Schmid-Tannwald C, Zwergal A, Niyazi M, Drexler M, Bartenstein P, Schnell O, Tonn JC, Thon N, Kreth FW, la Fougere C. Dynamic 18F-FET PET in newly diagnosed astrocytic low-grade glioma identifies high-risk patients. J Nucl Med. 2014;55(2):198-203.

127. Jansen NL, Suchorska B, Wenter V, Schmid-Tannwald C, Todica A, Eigenbrod S, Niyazi M, Tonn JC, Bartenstein P, Kreth FW, la Fougere C. Prognostic significance of dynamic 18F-FET PET in newly diagnosed astrocytic high-grade glioma. J Nucl Med. 2015;56(1):9-15.

128. Unterrainer M, Schweisthal F, Suchorska B, Wenter V, Schmid-Tannwald C, Fendler WP, Schuller U, Bartenstein P, Tonn JC, Albert NL. Serial 18F-FET PET Imaging of Primarily 18F-FET-Negative Glioma: Does It Make Sense? J Nucl Med. 2016;57(8):1177-82.

129. Guffens F MA, Van Laere K, Goffin K. Dynamic O-(2-18F-fluoro- ethyl)-l-tyrosine PET improves differentiation of local recurrent brain metastasis from radiation necrosis. J Nucl Med. 2015;56 (suppl 3):628.

130. Galldiks N, Langen KJ, Pope WB. From the clinician's point of view - What is the status quo of positron emission tomography in patients with brain tumors? Neuro Oncol. 2015;17(11):1434-44.

7. Statutory Declaration

"I, Winna Lim, by personally signing this document in lieu of an oath, hereby affirm that I prepared the submitted dissertation on the topic: *Differentiation of Tumor Recurrence from Radionecrosis Using 18F-FET-PET/CT after CyberKnife Radiosurgery of Brain Tumors* or *Differenzierung zwischen Tumorrezidiv und Radionekrose mittels 18F-FET-PET/CT nach radiochirurgischer Behandlung von Hirntumoren mit dem CyberKnife* independently and without the support of third parties, and that I used no other sources and aids than those stated.

All parts which are based on the publications or presentations of other authors, either in letter or in spirit, are specified as such in accordance with the citing guidelines. The sections on methodology (in particular regarding practical work, laboratory regulations, statistical processing) and results (in particular regarding figures, charts and tables) are exclusively my responsibility.

Furthermore, I declare that I have correctly marked all of the data, the analyses, and the conclusions generated from data obtained in collaboration with other persons, and that I have correctly marked my own contribution and the contributions of other persons (cf. declaration of contribution). I have correctly marked all texts or parts of texts that were generated in collaboration with other persons.

My contributions to any publications to this dissertation correspond to those stated in the below joint declaration made together with the supervisor. All publications created within the scope of the dissertation comply with the guidelines of the ICMJE (International Committee of Medical Journal Editors; www.icmje.org) on authorship. In addition, I declare that I shall comply with the regulations of Charité – Universitätsmedizin Berlin on ensuring good scientific practice.

I declare that I have not yet submitted this dissertation in identical or similar form to another Faculty.

The significance of this statutory declaration and the consequences of a false statutory declaration under criminal law (Sections 156, 161 of the German Criminal Code) are known to me."

_____ _____

Date Signature

Declaration of Contribution to Publication

Winna Lim contributed the following to the below listed publication:

Publication: Winna Lim, Gueliz Acker, Juliane Hardt, Markus Kufeld, Anne Kluge, Winfried Brenner, Alfredo Conti, Volker Budach, Peter Vajkoczy, Carolin Senger, Vikas Prasad,
Dynamic ^{18}F-FET PET/CT to differentiate recurrent primary brain tumor and brain metastases from radiation necrosis after single-session robotic radiosurgery.
Cancer Treatment and Research Communications, Volume 32, 2022, 100583, ISSN 2468-2942,
https://doi.org/10.1016/j.ctarc.2022.100583.
(https://www.sciencedirect.com/science/article/pii/S2468294222000739)

Contributions:

- Project administration
- Drafting and conceptualization of hypotheses and objectives
- Clinical database screening, exclusion and inclusion of study population
- Collection and organization of existing clinical and imaging data
- Assistance and data collection during expert analyses (nuclear medicinal and clinicoradiological)
- Analysis of the collected data
- Data visualization and processing of tables and graphics
- Writing of original draft and editing of manuscript post-review

_____

Signature, date and stamp of first supervising university lecturer

_____

Signature of doctoral candidate

Curriculum Vitae

Mein Lebenslauf wird aus datenschutzrechtlichen Gründen in der elektronischen Version meiner Arbeit nicht veröffentlicht.

Publication

Winna Lim, Gueliz Acker, Juliane Hardt, Markus Kufeld, Anne Kluge, Winfried Brenner, Alfredo Conti, Volker Budach, Peter Vajkoczy, Carolin Senger, Vikas Prasad: Dynamic ^{18}F-FET PET/CT to differentiate recurrent primary brain tumor and brain metastases from radiation necrosis after single-session robotic radiosurgery. Cancer Treatment and Research Communications, Volume 32, 2022, 100583, ISSN 2468-2942, https://doi.org/10.1016/j.ctarc.2022.100583. (https://www.sciencedirect.com/science/article/pii/S2468294222000739)

Acknowledgements

I thank Prof. Dr. med. V. Prasad, and Dr. med. M. Kufeld, from whom the idea of the study first initiated. I thank Prof. Dr. med. Dr. h.c. V. Budach and Prof. Dr. med. W. Brenner for their indirect support throughout this interdisciplinary study. I particularly thank Priv.-Doz. Dr. med. G. Acker, Prof. Dr. med. V. Prasad, and Dr. med. C. Senger for their time, patience, motivation, and supervision. Prof. Dr. med. V. Prasad provided much indispensable insight and guidance regarding all nuclear medicine aspects of this study. I especially thank Priv.-Doz. Dr. med. G. Acker for her support in the final stages of this work and for being an inspiring role model and main supervisor, whose mentoring was particularly essential for this dissertation. I thank Dipl.-Psych. J. Hardt not only for her professional guidance in statistics, but also for the motivation given. I thank the whole team at Charité CyberKnife Center, Charité Comprehensive Cancer Center, and technicians from the Department of Nuclear Medicine who helped in the process of data collection.

Last but not least, I am grateful to my parents and family for their hard work, endless support and sacrifice. Without them I would not be where I am today.

Confirmation by a Statistician

CHARITÉ

CharitéCentrum für Human- und Gesundheitswissenschaften

Charité | Campus Charité Mitte | 10117 Berlin

Institut für Biometrie und klinische Epidemiologie (iBikE)
Direktor: Prof. Dr. Geraldine Rauch
Postanschrift:
Charitéplatz 1 | 10117 Berlin
Besucheranschrift:
Reinhardtstr. 58 | 10117 Berlin
Tel. +49 (0)30 450 562171
geraldine.rauch@charite.de
https://biometrie.charite.de/

Name, Vorname: Winna, Winna
Emailadresse: winna.winna@charite.de
Matrikelnummer: 217073
Promotionsbetreuerin: Prof. Dr. Volker Budach
Promotionsinstitution/ Klinik: CC14 Klinik für Radioonkologie und Strahlentherapie CVK

Bescheinigung

Hiermit bescheinige ich, dass Frau Winna Winna innerhalb der Service Unit Biometrie des Instituts für Biometrie und klinische Epidemiologie (iBikE) bei Frau Dr. Juliane Hardt eine statistische Beratung zu einem Promotionsvorhaben wahrgenommen hat. Folgende Beratungstermine im Rahmen der Statistikambulanz wurden wahrgenommen:

- Termin 1: *17.10.2018*
- *Termin 2: 18.12.2018*
- Termin 3: *11.04.2019*

Folgende wesentliche Ratschläge hinsichtlich einer sinnvollen Auswertung und Interpretation der Daten wurden während der Beratung erteilt:

- Berücksichtigung von Auswertungsverfahren diagnostischer Studien entsprechend der klinischen Fragestellung
- Berücksichtigung der Abhängigkeit von Daten empfohlen (in jedem Fall methodische Diskussion der Abhängigkeit)

Diese Bescheinigung garantiert nicht die richtige Umsetzung der in der Beratung gemachten Vorschläge, die korrekte Durchführung der empfohlenen statistischen Verfahren und die richtige Darstellung und Interpretation der Ergebnisse. Die Verantwortung hierfür obliegt allein dem Promovierenden. Das Institut für Biometrie und klinische Epidemiologie übernimmt hierfür keine Haftung.

Datum: 29.06.2020

Name des Beraters/ der Beraterin: i.V. Dr. Dörte Huscher

[redacted]

Unterschrift Beraterin, Institutsstempel

CHARITÉ
UNIVERSITÄTSMEDIZIN BERLIN
Institut für Biometrie und Klinische Epidemiologie
Campus Charité Mitte
Charitéplatz 1 | D-10117 Berlin
Besucheranschrift: Rahel-Hirsch-Weg 5